Received: 17 February 2020 | Revised: 6 August 2020 | Accepted: 14 August 2020

DOI: 10.1111/bre.12507

ORIGINAL ARTICLE

Basin Research | IAS EAGE | WILEY

Reutilisation of hydrothermal vent complexes for focused fluid flow on continental margins (Modgunn Arch, Norwegian Sea)

Chantelle Roelofse[1] | **Tiago M. Alves**[1] | **Kamal'deen O. Omosanya**[2,3]

[1]3D Seismic Lab, School of Earth and Ocean Sciences, Cardiff University, Cardiff, UK

[2]Timelapsegeo AS, Trondheim, Norway

[3]formerly at Department of Geoscience and Petroleum, Norwegian University of Science and Technology, Trondheim, Norway

Correspondence
Chantelle Roelofse, 3D Seismic Lab, School of Earth and Ocean Sciences, Cardiff University, Cardiff, UK.
Email: roelofsec@cardiff.ac.uk

Funding information
Natural Environment Research Council, Grant/Award Number: GA/16S/007

Abstract

Conventional three-dimensional (3D) seismic data reveal abundant igneous activity on the Modgunn Arch, mid-Norwegian margin. Magmatic sills and associated hydrothermal vent complexes located at various depths prove the repeated utilisation of Paleocene-Eocene magmatic conduits. In total, 125 sills and 85 hydrothermal vent complexes were identified and mapped, with vent complexes ranging in diameter from 300 to 3,100 m and sills from 0.5 to 50 km. Three examples of stacked vent complexes are presented, revealing large eruptions of hydrothermal fluids vertically through the same conduit, from sills to the palaeo-sea floor. The vent complexes are found throughout Paleocene strata (66–56 Ma), whilst at least ten (10) vents were active during the Eocene. This study emphasises the importance of characterising ancient magmatic structures, as hydrothermal conduits and vent structures were, and may still be, reutilised as preferential fluid flow pathways to shallower strata. A minimum of four phases of hydrothermal vent complex formation are inferred. Cretaceous faults are both bypassed and used for magma and fluid flow. The reutilisation of magmatic structures here described may bring to light previously overlooked plays and renew interest in exploring magma-rich continental margins.

KEYWORDS

fluid migration, focused fluid flow, hydrothermal vent complexes, magma-rich margins, North Atlantic Ocean

1 | INTRODUCTION

Magmatic activity in sedimentary basins has a critical impact on all five elements of a petroleum system: maturation of source rocks, fluid migration, reservoir rocks, seals and traps (Holford, Schofield, MacDonald, Duddy, & Green, 2012; Rohrman, 2007; Senger et al., 2017). For example, magmatic intrusions in the Faroe-Shetland Basin acted as both barriers and carriers for hydrocarbons and other fluid, as crystalline intrusions may inhibit fluid flow and compartmentalise reservoir and source rocks (Senger et al., 2017). Conversely, fractured intrusions facilitate migration to shallow reservoirs (Rateau, Schofield, & Smith, 2013). Focusing on a different scope, Iyer, Schmid, Planke, and Millett (2017) modelled the temperature profile around magma intrusions in the Harstad Basin, offshore Norway, and demonstrated that source rocks can be overcooked in their vicinity. Conversely, source rocks considered to be too shallow for maturation may be heated into the oil window to produce hydrocarbons, but typically only in close proximity to the intrusions and for a limited time period during their cooling stages (Stagpoole & Funnell, 2001).

It is clear from the words above that magmatic activity adds much uncertainty and complexity to potential petroleum plays. Yet, large hydrocarbon fields may be discovered when magmatic elements work in favour of petroleum systems, such as the Rosebank Field, and Laggan and Tormore Fields in the Faroe-Shetland Basin (Duncan, Helland, & Dennehy, 2009; Schofield et al., 2017). Even when hydrocarbon potential has been hampered, hot intrusive rocks elevate the local geothermal gradient, turning an otherwise unprospective area into one posed for the development of geothermal energy (Bischoff, Nicol, Cole, & Gravley, 2019). Areas currently exploited for geothermal energy are related to young igneous systems, Quaternary volcanism and shallow (<6 km) magmatic intrusions, as in the case of Iceland (Stimac, Goff, & Goff, 2015). Other regions with elevated geothermal gradients, possibly due to a thinned crust inherited from continental rifting (e.g. North Sea), are becoming increasingly important. Elgin and Franklin are examples of high pressure, high temperature hydrocarbon fields in the North Sea from which heat could be used to generate electricity on oil and gas platforms (Lockett, 2018).

Hydrothermal vent complexes (HTVCs) formed due to the expulsion of gases and fluidised material are associated with the emplacement of igneous intrusions in sedimentary basins (Kjoberg et al., 2017; Omosanya et al., 2018; Reynolds et al., 2017; Svensen, Jamtveit, Planke, & Chevallier, 2006; Svensen, Planke, Jamtveit, & Pedersen, 2003). Supra-sill strata are often fractured at the tips of magmatic sill complexes due to the build-up of overpressure associated with the release of fluids and gases within metamorphic aureoles (Jamtveit, Svensen, Podladchikov, & Planke, 2004; Omosanya et al., 2018). Fluids migrate towards the sea floor through fractured conduits to form HTVCs. These typically occur in basins that experience crustal extension with considerable magmatic input, for example, the Karoo Basin in South Africa (Svensen et al., 2006), magma-rich continental margins such as the Bass Basin offshore Australia (Holfor, Schofield, & Reynolds, 2017), or the Vøring and Møre Basins offshore mid-Norway (Planke, Rasmussen, Rey, & Myklebust, 2005; Skogseid Pedersen, Eldholm, & Larsen, 1992). Hence, rift basins and resulting continental margins are commonly categorised as magma-rich or magma-poor, with magma-rich margins being associated with: a) higher spreading rates than their magma-poor counterparts, and b) large volumes of syn-rift igneous rocks (Franke, 2013; White & McKenzie, 1989). Large Igneous Provinces (LIPs) such as the North Atlantic Igneous Province, form in such magma-rich continental margins (Bryan & Ernst, 2008).

This study focuses on the southern part of the Modgunn Arch, a N-S trending Paleogene dome in the southern Vøring Basin with ample evidence of magmatic activity during the early Cenozoic (Manton, 2015; Miles & Cartwright, 2010). Sills are imaged in seismic reflection data as saucer-shaped or sheet-like, high-amplitude reflections that cross-cut the host-rock strata, caused by an increase in acoustic impedance with depth (Hansen & Cartwright, 2006b). In comparison, hydrothermal vent complexes are imaged as pipe-like, vertical zones of low amplitude and chaotic reflections in the conduits, terminating as dome, eye-shaped or crater morphologies at their summits (Hansen, 2006; Omosanya et al., 2018). Based on the stratigraphic position of upper terminations in the HTVCs, Hansen (2006) and Planke et al. (2005) used the close relationship between the latter vent complexes and underlying sills to estimate the timing of sill intrusion. They considered the North Atlantic Volcanic Province in the Vøring and Møre Basins to have been emplaced from the Paleocene to Eocene; the volcanic gases subsequently released from the HTVCs during this time are considered to be the cause of the major climate change event known as the Paleocene-Eocene Thermal Maximum (Aarnes, Planke, Trulsvik, & Svensen, 2015).

Radiometric dating of sills to estimate the duration of intrusions can be somewhat erroneous due to subsequent alteration processes of intruded magma and to the poor sampling usually provided by exploration boreholes (Gibb & Kanaris-Sotiriou, 1988). Knowing this, Hansen and Cartwright (2006a) used post-intrusion sediment distribution and onlap relationships in seismic data to calculate the timing of sill intrusions. Hansen (2006) stated that the formation of HTVCs occurs within the time it takes for an intrusion to cool, with very thick (>300 m) sills solidifying within 10 ka (Jaeger, 1958). This timeframe is much faster than the resolution obtained from seismic interpretation, which Hansen (2006) demonstrated to have a minimum uncertainty of >100 ka. In a subsequent study, Svensen, Planke, and Corfu (2010) dated the Pb-U ages in zircons from two mafic sills in well 6607/5-2, to 55.6 ± 0.3 Ma and 56.3 ± 0.4 Ma, which proved to be more precise than previous methods of dating sills using K-Ar (Gibb & Kanaris-Sotiriou, 1988). In addition, Hafeez et al. (2017) used Ar-Ar dating on igneous samples offshore mid-Norway, which yielded dates of 57–58 Ma.

Highlights

- 3D Seismic interpretation reveals stacked hydrothermal vent complexes on the Modgunn Arch.
- Hydrothermal vent complexes have been reutilised as fluid-focusing pathways.
- Faults and hydrothermal vent complexes alternate as main pathways for magma and fluid.
- At least four phases of magmatic intrusion are interpreted across the Paleocene and Eocene on the Modgunn Arch.

The properties of the acquired seismic signal make it impossible to obtain absolute ages for discrete distinct intrusive events based solely on seismic data, as slightly diachronous HTVCs may share the same basal and upper vent boundaries. Nevertheless, the relative timing of HTVCs and their intrusions can be inferred when using relatively high-quality seismic data to image different stratigraphic levels, as demonstrated in this paper. As core and physical rock samples from sills are not commonly collected by wells, seismic relationships are still a useful tool for assessing the relative timing of intrusions. For instance, Holford et al. (2017) and Svensen et al. (2003) presented examples of HTVCs focusing fluid migration to shallower units in the Bass and Vøring Basins, respectively, long after the intrusions happened. Against such a background, the research questions of this study are as follows:

1. How many distinct magmatic events are recorded on the Modgunn Arch, and how extensive are these events on a magma-rich margin such as offshore mid-Norway?
2. Are hydrothermal vent complexes fed by specific types and depths of sills?
3. What are the implications of reutilising magma migration pathways on the local petroleum systems, at the scale of a hydrocarbon- or geothermal prospect?

2 | GEOLOGICAL FRAMEWORK

2.1 | Tectonic evolution of the Modgunn Arch

The Norwegian margin has undergone several phases of extension and compression since the Late Paleozoic. Prior to this, orogenic events such as the Caledonian Orogeny established the NE-SW structural trend of the Vøring and Møre Basins in the Norwegian Sea (Doré, Lundin, Fichler, & Olesen, 1997). The Vøring and Møre Basins are Cretaceous in age and were predominantly filled by marine sediment. They are 400–500 km long and separated by the Jan Mayen Corridor, an extension of the Jan Mayen Fracture Zone (Brekke, Dahlgren, Nyland, & Magnus, 1999). The Modgunn Arch is located above the Jane Mayen Corridor, at the boundary between the Vøring and Møre Basins, ~370 km west of Trondheim (Figure 1).

Three main phases of rifting formed the mid-Norwegian margin: (a) Permian to Early Triassic, (b) Late Jurassic to Early Cretaceous, and (c) Late Cretaceous to Paleocene (Gómez & Vergés, 2005). In the study area, Late Cretaceous – Paleogene continental rifting was accompanied by widespread magmatic intrusion of sills and associated hydrothermal vent complexes into thick Cretaceous strata (Omosanya et al., 2018; Planke et al., 2005; Svensen et al., 2003). The intrusions are directly linked to continental breakup and oceanic crust formation between Norway and Greenland at ~55 Ma, close to the Paleocene-Eocene boundary (Lundin & Doré, 2002). On the Modgunn Arch per se, the presence of igneous rocks is confirmed by a 1-m thick sill unit encountered in well 6403/6-1 (Manton, 2015). Magmatic intrusions are evident throughout the Cretaceous and Paleocene strata (Figures 2, 3) as positive high-amplitude, saucer-shaped and planar-transgressive seismic reflections cross-cutting host strata.

After continental breakup, a combination of mid-Cenozoic compressional doming, basin inversion along the Jan Mayen Corridor, and local differential compaction, resulted in the formation of the Modgunn Arch as observed at present, which is roughly oriented north-northwest to south-southeast (Brekke, 2000; Gómez & Vergés, 2005). Using stratigraphic relationships, Brekke (2000) suggested that the Modgunn Arch formed in the Middle Miocene at the same time as the neighbouring Helland-Hansen Arch.

The Plio-Pleistocene records widespread glaciation and subsequent progradation of clastic sediments along the mid-Norwegian margin (Hjelstuen, Eldholm, & Skogseid, 1999). Several submarine landslides occurred across the Norwegian margin in response to glacial advance and retreat. In the southern part of the Modgunn Arch, Song, Alves, Omosanya, and Ze (2020) correlated the location of recent submarine slides to the distribution of underlying faults, and suggested that fluid migration along these faults weakened the overlying strata, leading to slope instability over the arch.

2.2 | Stratigraphy of the Modgunn Arch

In this work, stratigraphic data for the Vøring and Møre Basins are based on the Norwegian Petroleum Directorate (NPD) lithostratigraphic chart from 2015 (Figure 2). Lithostratigraphic information specific to the study area is provided by the Edvarda well 6403/6-1 (Figure 3). This exploration well reached a depth of 4,120 m, penetrating the Quarternary Naust Formation near the sea floor to terminate in the Lysing Formation, part of the Upper Cretaceous Cromer Knoll Group (Dalland, Worsley, & Ofstas, 1988) (Figure 2).

The Lysing Formation consists of white-grey sandstones deposited by deep-marine fans. Overlying the Lysing Formation are the Kvitnos, Nise and Springar Formations, which make up the Shetland Group (Upper Cretaceous). The three latter units consist of calcareous claystones interbedded with minor carbonates and sandstone stringers, reflecting deposition in open marine environments (Dalland et al., 1988). The Nise Formation contains a greater proportion of sand when compared to the rest of upper Cretaceous strata, consisting of interbedded sandstones, siltstones and shales (Dalland et al., 1988).

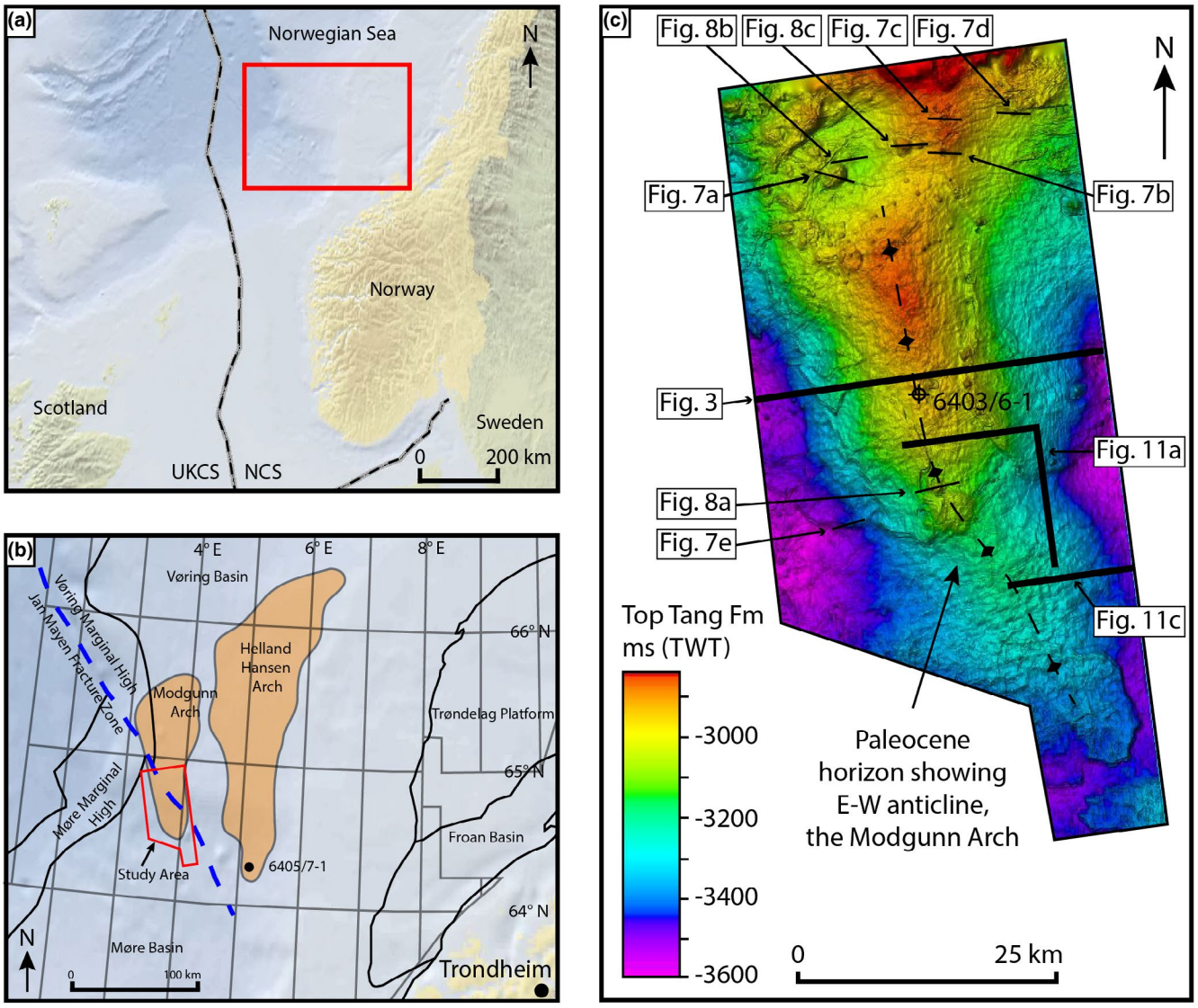

FIGURE 1 (a) Map of the Norwegian Sea. (b) Location of study area in the southern part of the Modgunn Arch, highlighting main structural elements in the Vøring and Møre Basins. (c) Top Tang Formation (Paleocene) showing an anticlinal structure where well 6403/6-1 was drilled, and the locations of seismic sections shown in this study

An unconformity separates Cretaceous strata from the Paleocene Rogaland Group, which was also deposited in a deep-marine environment. The Tang and Tare Formations consist of claystones with minor sandstone and limestone; the Tare Formation contains variable amounts of volcanic tuffs. Tuff content increases towards the base of the unit, reflecting high volcanic output during this time (Kjoberg et al., 2017; Schmiedel et al., 2017). The Tare Formation is equivalent to the Balder Formation in the North Sea (Dalland et al., 1988; Deegan & Scull, 1977).

The deep-marine, claystone-dominated Brygge Formation of the Hordaland Group overlies the Rogaland Group and was deposited during the Eocene to early Miocene (Figure 2). The Kai Formation of the Nordland Group (early Miocene to late Pliocene) contains alternating claystone, siltstone and sandstone with limestone stringers, all deposited in a marine environment (Dalland et al., 1988). In contrast, a thick, prograding clastic wedge was deposited across the mid-Norwegian margin from the late Pliocene-early Pleistocene as a result of the Northern Hemisphere glaciation and tectonic uplift of Fennoscandia (Gómez & Vergés, 2005; Hjelstuen et al., 1999). This unit is present on the Modgunn Arch as the 40-m thick Naust Formation.

2.3 | Petroleum systems of the Vøring and Møre basins

Brekke et al. (1999) summarised the hydrocarbon potential of the Vøring and Møre Basins. They noted that the main uncertainty for prospectivity in the two basins is the presence and maturity of organic-rich source rocks, although a regional transgression during the Late Jurassic resulted in the deposition of a source rock akin

to the Kimmeridge Clay Formation (Underhill, 1998). Cretaceous sandstones with reservoir potential are considered to be present, but may not be laterally extensive (Brekke et al., 1999). However, if charged by a Cretaceous source rock, these reservoirs could form a promising play, particularly if located within anticlinal or fault traps such as on the Modgunn Arch (Brekke et al., 1999).

A successful Paleocene play consisting of an early Paleocene sandstone reservoir, a Tertiary domal trap and an unknown thermogenic source, is present towards the Trøndelag Platform area of the Møre Basin (Brekke et al., 1999). The Paleocene play could also be successful elsewhere on the Norwegian margin, but requires either hydrocarbon migration from potential Cretaceous sources or re-migration from older source rocks (Brekke et al., 1999). No hydrocarbon fields on the Modgunn Arch have been discovered to date and the presence of volcanics makes the study area difficult to explore; the high chance of drilling into volcanic rocks turns the prospect economically costly and technically challenging.

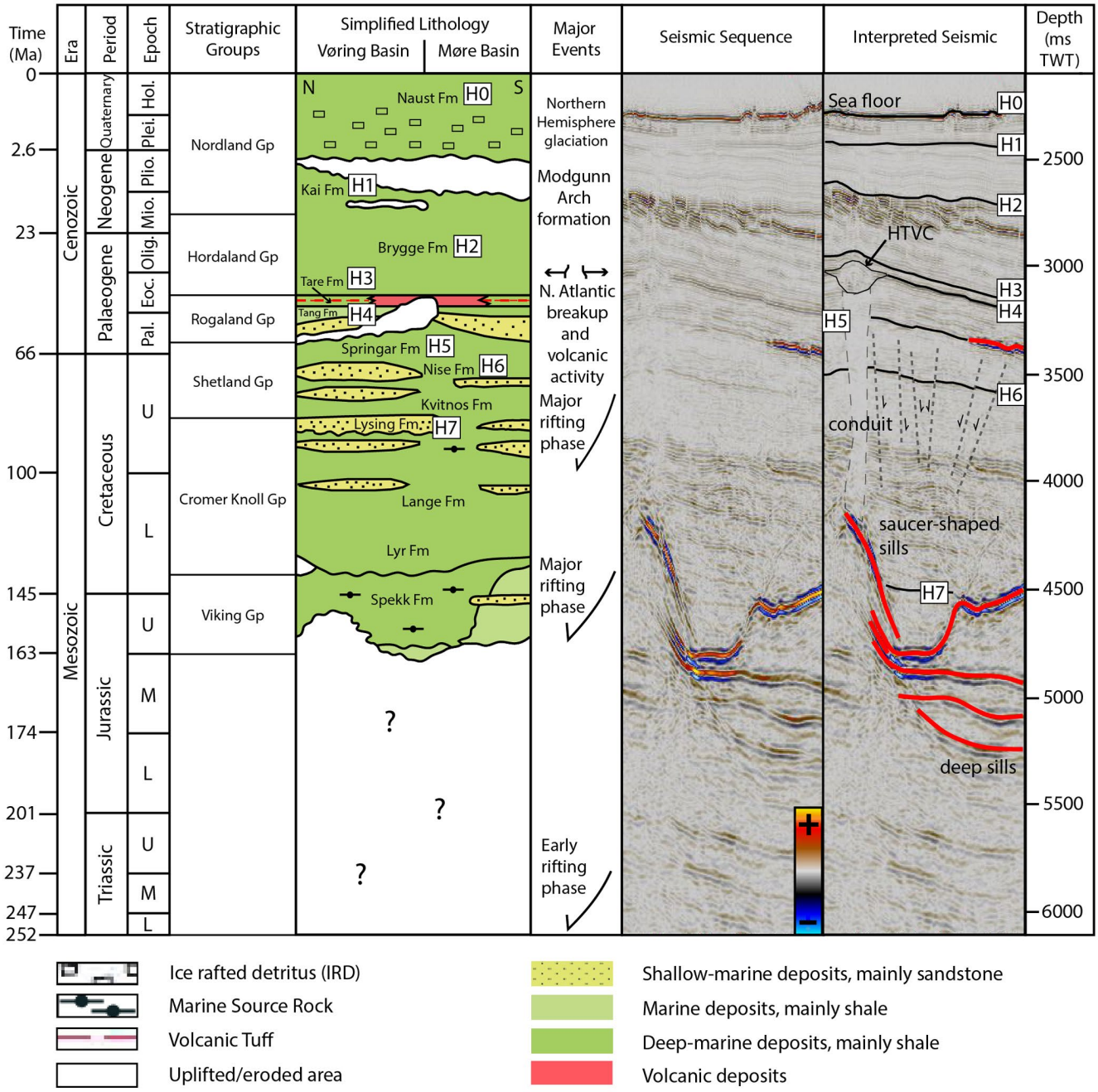

FIGURE 2 Stratigraphic framework of the Modgunn Arch. Representative seismic interpretation is shown on the right, with seismic horizons labelled H1–H7. Modified after 'The, 2014 NPD lithostratigraphic charts' (2014). HTVC, hydrothermal vent complex

3 | DATA AND METHODS

3.1 | Interpreted database

The 3D seismic reflection survey interpreted in this study is located offshore mid-Norway, on the southern part of the Modgunn Arch (Figure 1). The survey MC3DMGS2002 covers an area of 2,635 km^2 and was acquired in 2002 by PGS. The survey was processed as a zero-phase, 3D volume displayed following the European polarity such that an increase in acoustic impedance with depth is shown as a red positive peak, whilst troughs are coloured blue (Figure 2). Inlines and crosslines are oriented NNW and WSW respectively, processed to a bin spacing of 12.5 m. The seismic cube is presented in two-way time (TWT) with a vertical sampling rate of 4 milliseconds two-way time (ms TWT). Water depth ranges from 1,100 m to 2,100 m, deepening to the west.

Well 6403/6-1 was drilled in 2006 in the centre of the southern Modgunn Arch to test for hydrocarbons in the Upper Cretaceous (Campanian) Nise and Lysing Formations, as well as putative reservoirs in Paleocene and Maastrichtian strata (Factpage6403/6-1, 2008). Although traces of migrated hydrocarbons were interpreted from post-well geochemical analyses in side-wall cores from the uppermost Nise Formation, there were no hydrocarbon shows in the Nise or Lysing Formations. Sandstones were tight and the well was abandoned (Factpage6403/6-1, 2008). Borehole-seismic correlations indicate that the vertical seismic resolution is ~8 m in the Brygge to Naust Formations (i.e. in post-breakup units dated as Late Eocene to Quaternary). Vertical seismic

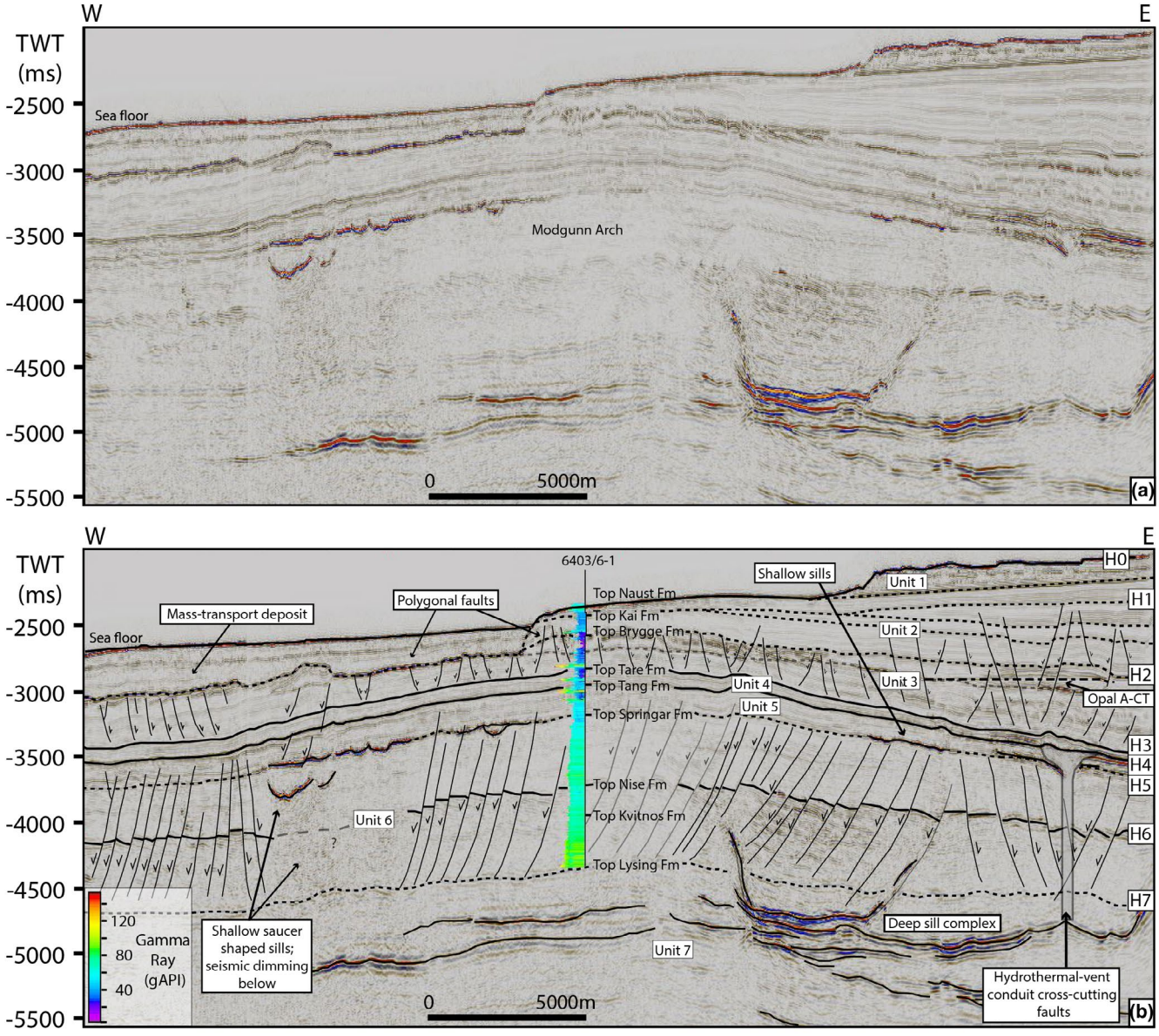

FIGURE 3 (a) Uninterpreted and (b) interpreted representative seismic profile E-W across the Modgunn Arch showing well 6403/6-1 with its gamma ray curve and labelled well tops. Seismic units 1–7 and seismic horizons H0–H7 are labelled in the figure. Location of seismic profile shown in Figure 1

resolution approaches 17 m in the Tare and Tang Formations, 29 m in the Springar Formation, and 36–40 m in strata spanning the Nise to Top Lysing Formations.

3.2 | Seismic interpretation of horizons and sills

Schlumberger's Petrel® was used to complete the high-resolution seismic mapping of 125 magmatic sills and three key seismic horizons tied to well 6403/6-1: the Top Tare Formation, Top Tang Formation and Top Nise Formation (Figure 3). The three seismic horizons were interpreted in detail on vertical (2D) seismic sections using a 2D-autotracking picking tool. A grid of 50 × 50 inlines and crosslines was interpreted and considered as the basic interpretation nodes, with more closely spaced mapping attained in complex areas, after which a 3D interpolation tool in Petrel was applied and high-quality surfaces were generated in map view. The quality of the Top Nise Formation seismic reflection varied considerably throughout the study area due to seismic dimming by overlying sills. In these areas, the Nise Formation is assumed to be present but it was not seismically interpreted (Figure 3). Thickness variations occur in the Tare Formation due to differential compaction over intrusion-related structures (Kjoberg et al., 2017; Song et al., 2020). Thus, the regional unconformity at the top of the Top Tang Formation (late Paleocene) was used as a reference horizon for interpreting the relative ages of the hydrothermal vent complexes (Figure 1c).

Sills are imaged in seismic data as high-amplitude, positive seismic reflections due to their greater density and P-wave velocity when compared to host strata (Hansen & Cartwright, 2006b; Senger et al., 2017; Smallwood & Maresh, 2002). Diagnostic features in sills include their abrupt reflection terminations, saucer shapes and cross-cutting geometries in host strata (e.g. Planke et al., 2005, 2015). These characteristics were used in conjunction with their high-amplitude nature to identify and map sills in the three dimensions. The sills were interpreted in 2D seismic sections using both manual and 2D-autotracking picking tools in a 5x5 inline and crossline grid, after which polygons were drawn in map view around each sill, and corresponding surfaces were generated. Each sill was classified into one of three categories according to their relative depth of emplacement: (a) shallow sills within the lowermost Tang and Springar Formations, (b) medium-depth sills within the Nise and Kvitnos Formations and (c) deep sills in the Lysing Formation and deeper strata. Based on well 6403/6-1, shallow sills occur at a depth between 2,400 and 3,048 m, medium-depth sills occur at a depth between 3,048 and 4,018 m, and the deepest sills are below 4,018 m. Well 6403/6-1 was drilled right in the centre of the southern part of the Modgunn Arch, so these depths increase to the east, west and south along the flanks of the arch as the strata have been folded after sills were intruded.

Schofield et al. (2017) showed that as many as 88% of the sills penetrated by wells in the Faroe-Shetland Basin were less than 40 m in thickness; therefore, although 125 sills were mapped in this study area, it is expected that more sills exist well below the seismic resolution of the interpreted 3D volume, that is, the sills are tuned reflections. Also, the convoluted nature of sill intrusions hinders the identification of discrete sills in parts of the study area. However, the presence of a dense population of sill complexes is clear in seismic data (Figure 3).

3.3 | Seismic interpretation of hydrothermal vents

Hydrothermal vent complexes were identified in seismic data as vertical zones of low amplitude and chaotic reflections in the conduits terminating close to the Top Tang Formation, forming 'crater', 'dome' and 'eye-shaped' vents. The interior of the vents vary between chaotic seismic reflections and clear reflections that terminate within the vents. These morphologies were used to classify the HTVCs following the methodology in Planke et al. (2005) and Hansen (2006). Due to the variation in depth of the vents, a regional 'top vent' or 'base vent' horizon was not interpreted, but the tops and bases of the vents were still identified for each HTVC according to the recognition of: a) where outer-vent reflections were truncated against (revealing the base vent reflection), b) onlapping reflections onto the vents (defining the top of the vent), and c) reflections continuing beyond the diameter of the vent, such as above a crater or below a dome (Figure 4). Polygons were drawn in map view around the HTVCs and their areas were computed in Petrel®, from which HTVCs diameters were calculated and compared across different structures. Furthermore, the height of the HTVCs was measured in ms (TWT), and depth converted using a seismic velocity of 1,800 m/s for vent interior, as used by Planke et al. (2005), derived from well 6607/12-1. The relative timing of formation of HTVCs was determined using a similar methodology to Alves (2012) by measuring the number of seismic reflections from the base vent horizon above or below the Top Tang Formation, and their distribution was plotted on a bar plot across four sectors of the Modgunn Arch. In our method, the presence of high-amplitude anomalies or seismic dimming in the strata overlying the HTVCs was plotted relative to the Top Tare Formation, as they possibly indicate later stages of fluid flow. Sills were plotted relative to the Nise and Lysing Formations. However, as the seismic reflectivity of host strata diminishes with depth, the approximate thickness of the sill complex or thickness of the strata crossed by a sill is represented in ms TWT instead of the number of seismic reflections as in Alves (2012). This thickness is measured to the nearest 50 ms TWT. As the interpretation of sill complexes is limited by

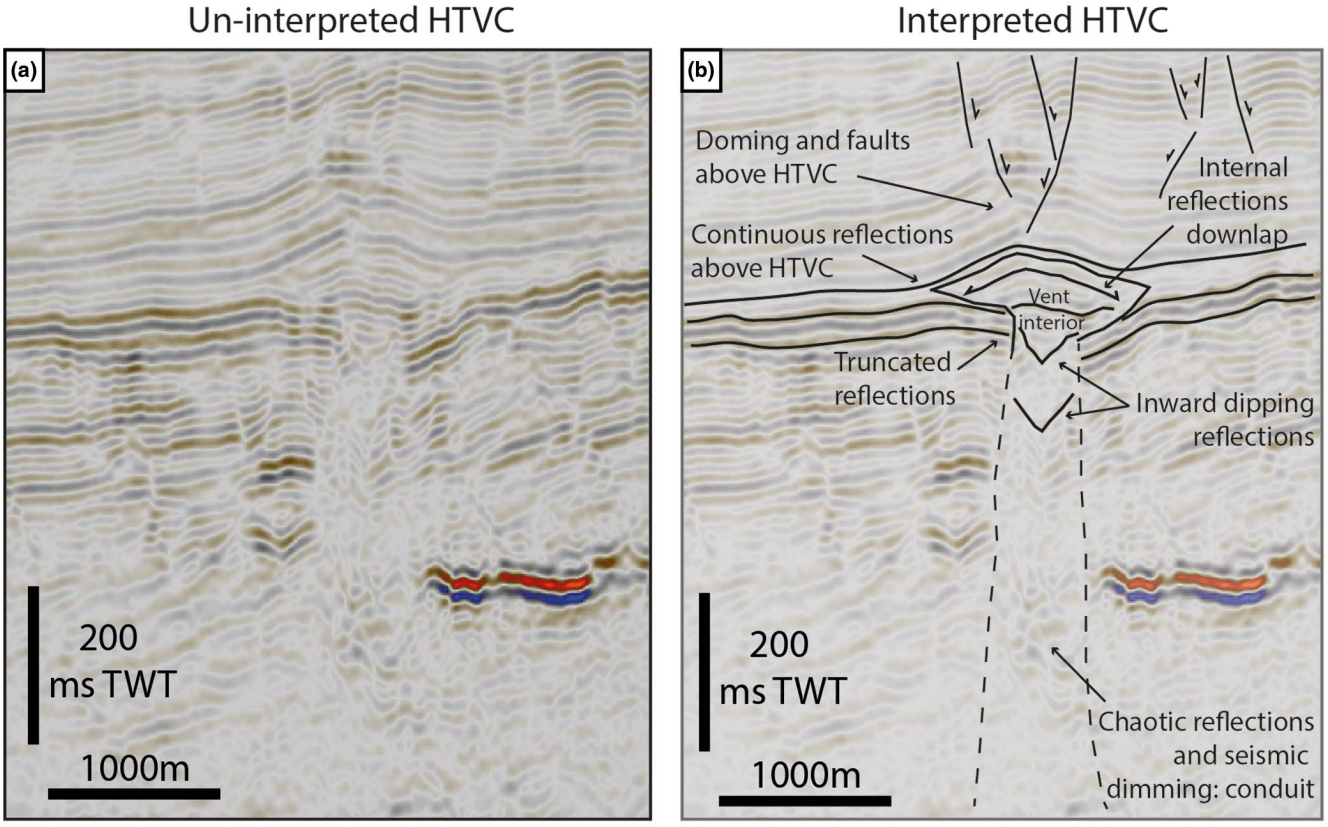

FIGURE 4 Example of an un-interpreted (a) and interpreted (b) hydrothermal vent complex, highlighting seismic reflection characteristics. Further examples of the different vent types are given in Fig. 7.

seismic resolution, the thicknesses are not assumed to be accurate, but relative across the study area.

The root mean square (RMS) amplitude attribute was extracted in a 100 ms TWT window across the Nise Formation horizon to reveal amplitude anomalies that may correspond to fluid flow.

4 | SEISMIC STRATIGRAPHY

The study area comprises seven seismic-stratigraphic units (Figure 3; Appendix A). The horizons delimiting main stratigraphic units (and their relative ages) are determined from the stratigraphic tops in well 6403/6-1. Unit 1 consists of chaotic internal strata bound by an irregular sea floor and a relatively planar base (H1), suggesting the presence of a mass-transport deposit. Unit 2 (bounded by horizons H1 and H2) consists of the Kai Formation and forms a wedge of planar strata with internal onlapping geometries displaced by a shallow tier of faults that extend down to Unit 3. Unit 3 (bounded by horizons H2 and H3) correlates with the Brygge Formation and is faulted, showing multiple local onlap and truncation geometries, with laterally discontinuous amplitudes ranging from seismic dimming to high-amplitude, positive anomalies, in places associated with underlying faults or HTVCs. A positive amplitude seismic reflection cross-cuts this unit in the northeast of the study area, corresponding to a 'fossil' Opal A-CT phase boundary (Brekke et al., 1999). Unit 4 (bounded by horizons H3 and H4) correlates with the Tare Formation and consists mostly of planar seismic reflections with local high-amplitude anomalies, onlap and thickness changes above HTVCs. Horizon H3 (Top Tare Formation) comprises a positive, medium-amplitude seismic reflection, whilst horizon H4 (Top Tang Formation) is a positive, high-amplitude seismic reflection that shows slight lateral variations in amplitude as this reflection is an unconformity. Both of these horizons were seismically mapped across the study area.

Unit 5, spanning from H4 to H5, consists of planar seismic reflections with occasional onlapping relationships. It contains HTVCs with chaotic internal seismic characters, whilst external seismic reflections either onlap onto the HTVCs or are truncated against them (Figure 4). Below HTVCs, and at the base of this unit, are locally very high amplitude, positive seismic reflections corresponding to igneous intrusions. These are typically saucer-shaped but also planar transgressive and layer-parallel (Planke et al., 2005).

Unit 6 (bounded by horizons H5 and H7) and Unit 7 (below horizon H7) are mostly seismically transparent, but large faults at least 1 s TWT in height offset them. Horizon

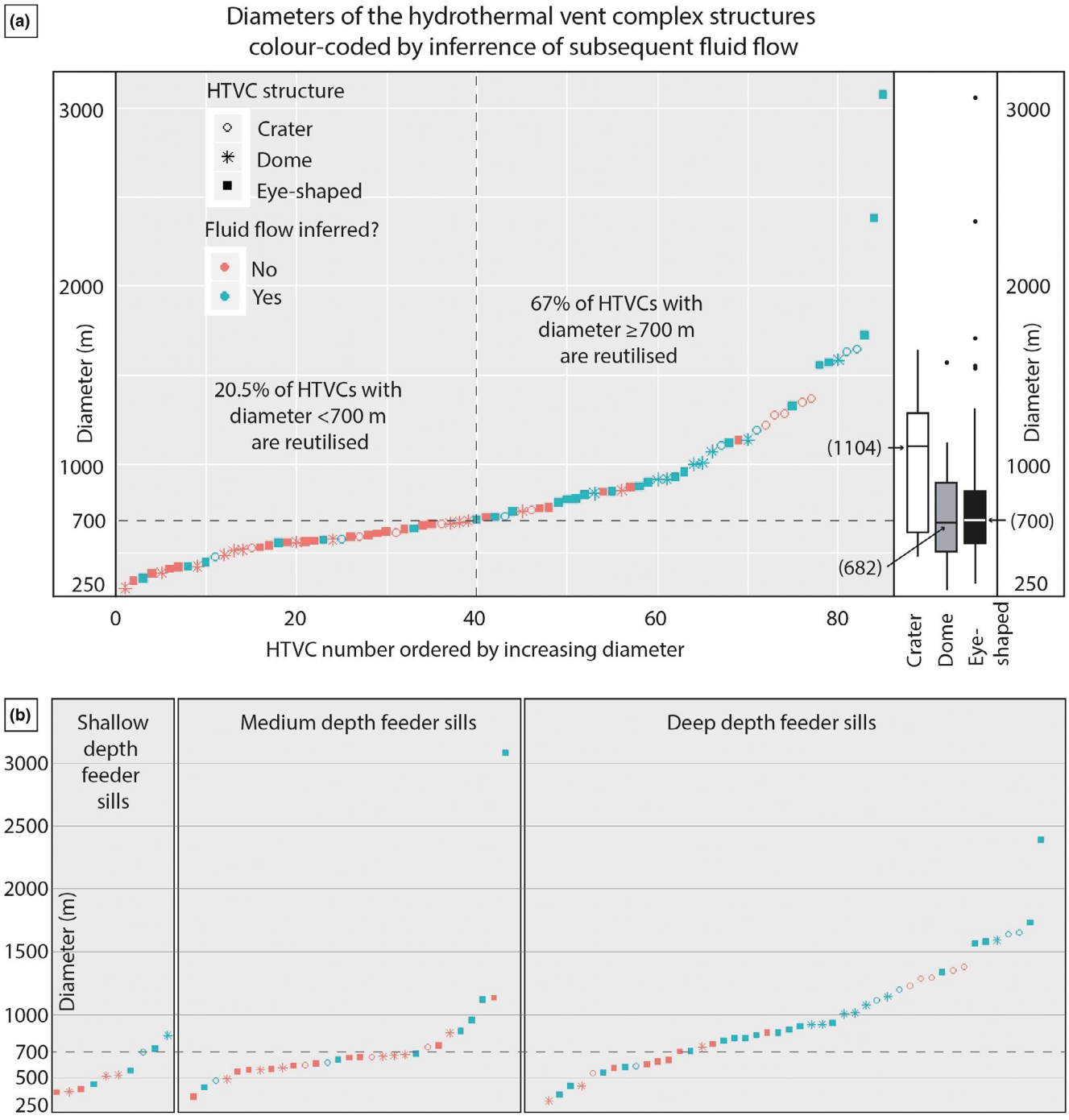

FIGURE 5 (a) Graphic representation of the range of the diameter of HTVCs, ordered by increasing diameter (scatter plot) and by structure (box plots). The colours represented in the scatter graph reflect the positive (or negative) inference of subsequent fluid flow from amplitude anomalies above HTVCs. The box plots show the range in the diameter of HTVCs, with median values in brackets. The plots show that craters are on average larger features compared to the domes and eye-shaped HTVCs. Generally, the larger HTVCs are reutilised by fluid. (b) Diameter of HTVCs divided into three groups according to the depth of the feeder sill feeding the HTVC: shallow, medium and deep depth, with the same symbol key as (a)

H6 (Top Nise Formation) is a densely faulted, negative seismic reflection. Its amplitude is low, but still relatively high compared to the surrounding stratigraphy; it was, therefore, possible to map this horizon across the study area, except in areas where seismic dimming prevented a reliable interpretation. Igneous intrusions are present, are characteristically saucer-shaped in Unit 6, whilst those in Unit 7 have planar transgressive or layer-parallel geometries (Figure 3).

5 | SEISMIC INTERPRETATION OF MAGMATIC FLUID FLOW FEATURES

5.1 | Morphology of hydrothermal vent complexes

The HTVCs are circular to oval-shaped in plan view and their average diameter ranges from 300 to 3,100 m (Figure 5),

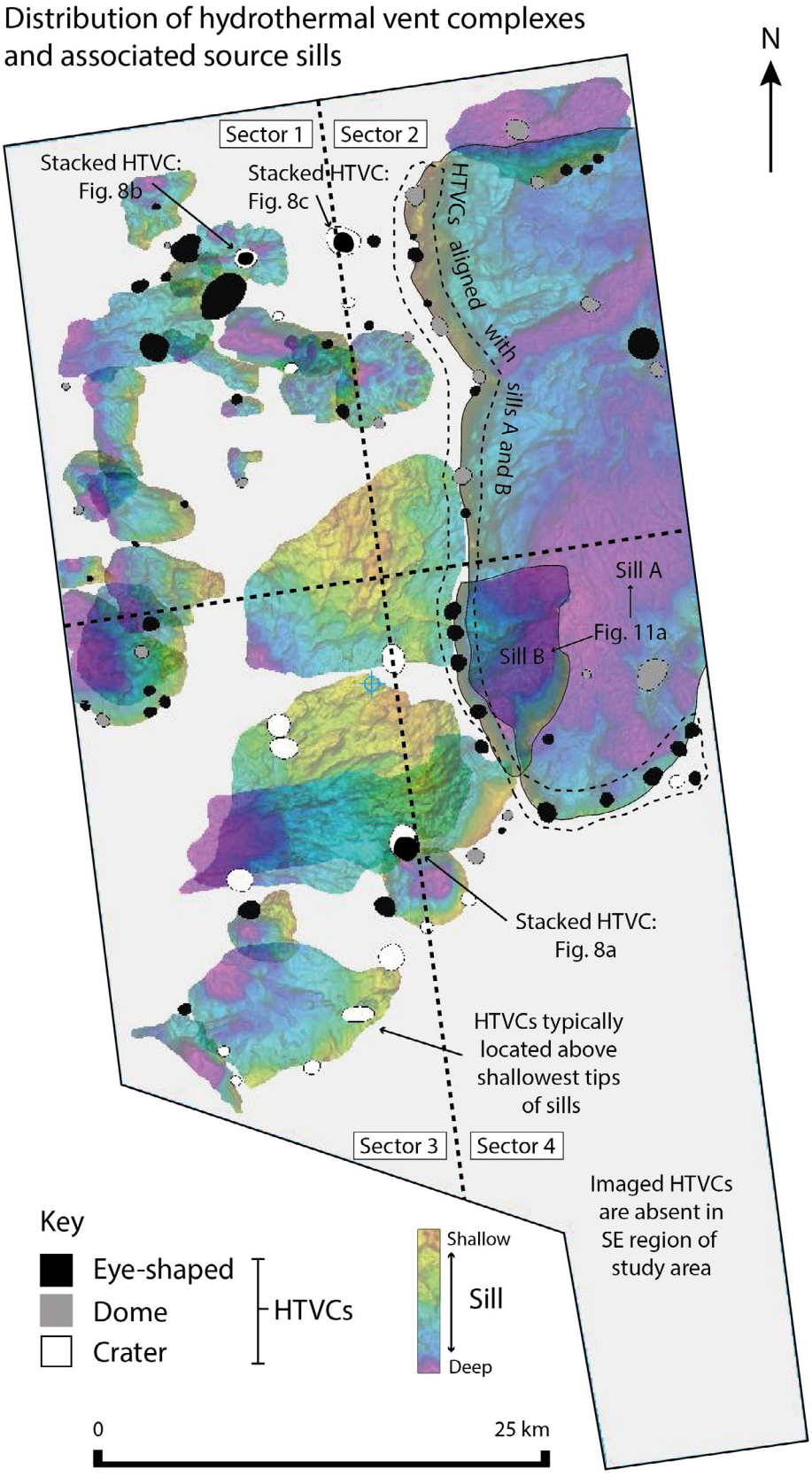

FIGURE 6 Map showing the distribution of 85 hydrothermal vent complexes, coloured by structure, and the 27 source sills mapped in this work. In the study area, 20 HTVCs are aligned with the 50 km N-trending sill on the eastern flank of the Modgunn Arch. The four sectors shown in Figure 9 are labelled on the map.

whilst the approximate height of the HTVCs range between 27 and 374 m. These scales are similar to those interpreted offshore Greenland and elsewhere offshore Norway, along the North Atlantic margin (Table 1).

The craters are generally wider than the domes and eye-shaped HTVCs, recording a median diameter of 1,104 m, compared to 682 m and 700 m for domes and eye-shaped vents, respectively. Of the 85 hydrothermal vent complexes

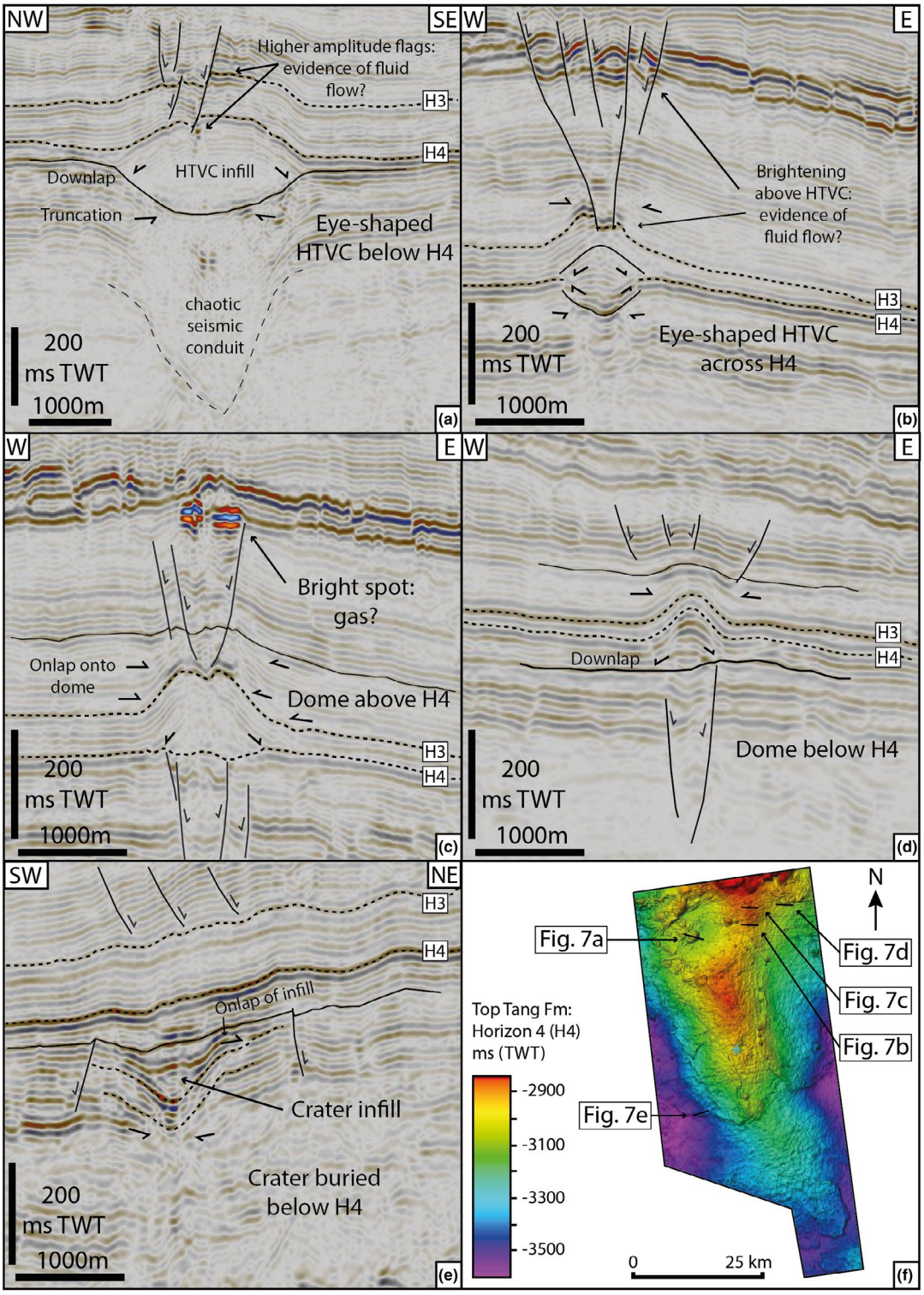

FIGURE 7 Examples of the different structural types of HTVCs relative to Horizon 4 (Top Tang Formation): a) eye-shaped below H4; b) eye-shaped across H4; c) dome above H4; d) dome below H4; e) crater below H4; f) Time-structure map of the Top Tang Formation with locations of the HTVCs shown in Figures 7a to 7e.

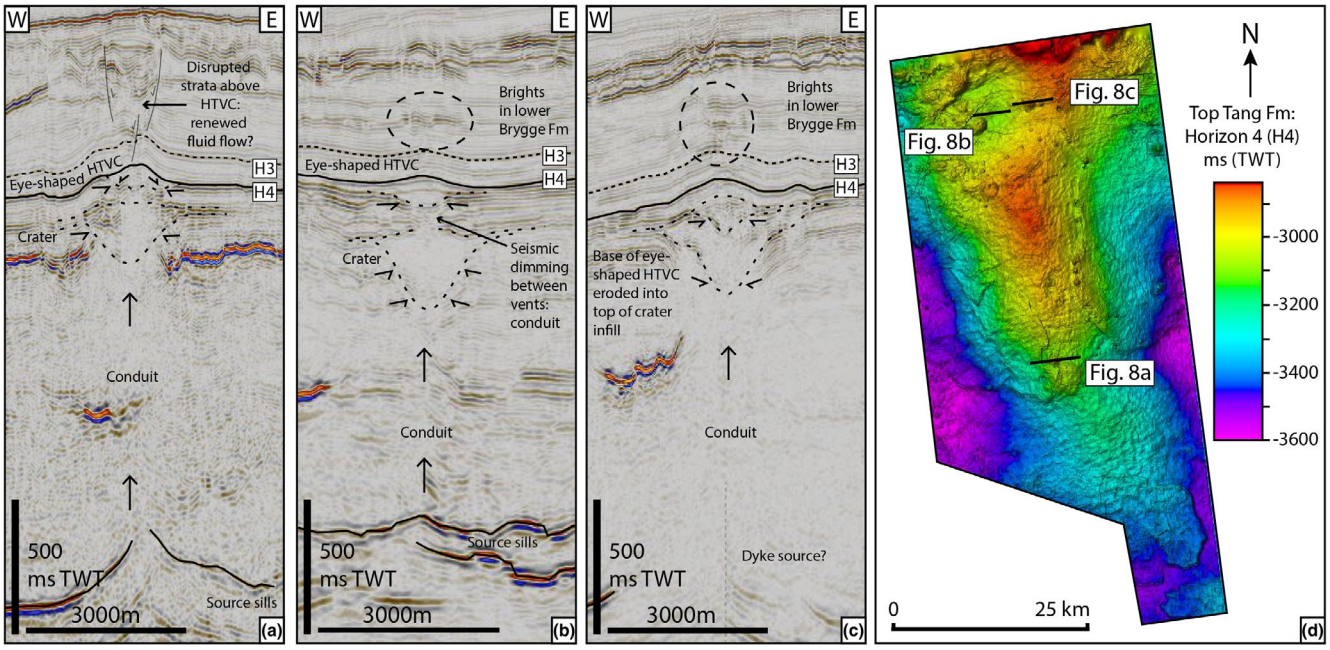

FIGURE 8 Seismic examples of stacked HTVCs and those with overlying high amplitude anomalies. (a) Crater HTVC located six seismic reflections below the Top Tang Formation, with an eye-shaped HTVC above at the Top Tang Formation horizon. Seismic dimming is observed through the HTVCs and faulted strata above, possibly indicating renewed fluid flow. (b) Crater HTVC located 12 seismic reflections below the Top Tang Formation, with an eye-shaped HTVC located at the Top Tang Formation. Bright spots in the overlying strata suggest later fluid migration. (c) Crater HTVC located four seismic reflections below the Top Tang Formation, with an eye-shaped HTVC at the top of the crater fill, indicating a second phase of HTVC formation immediately after the crater was filled. It is interpreted that the lack of clear source sills and presence of vertical seismic disruptions indicate that a vertical dyke fed the HTVCs. (d) Top Tang Formation with locations of seismic examples

mapped in the study area 17 are craters, 21 are domes and 47 are eye-shaped vents. These HTVCs are distributed across the Modgunn Arch directly above the tips of stratigraphically deeper source sills (Figure 6). Out of 125 mapped sills, 27 sills (22%) feed shallower HTVCs. The source sills range in diameter from 1 to 50 km, that is,the presence of HTVCs does not appear to be dependent on the size of the sills. Of the 27 source sills four are shallow sills, 13 are medium-depth sills, and 10 are deep-seated sills. All of the sills are associated with five or fewer HTVCs, apart from two sills on the eastern flank of the Modgunn Arch where a large deep sill extending for at least 50 km in a N-S direction appears to feed 20 HTVCs along its rim (Sill A). Another discrete sill (Sill B) on the eastern flank feeds seven HTVCs (Figure 6). These sills are interpreted to be spatially coincident with a deep crustal fault, which was likely the source for the sill complex and magmatic fluids.

5.2 | Distribution of hydrothermal vent complexes and associated seismic anomalies

Figures 7 and 8 show examples of different structures and levels of HTVCs in seismic section. The spatial and temporal distribution of HTVCs across four sectors of the Modgunn Arch is shown by the bar plots in Figure 9. The locations of amplitude anomalies, seismic dimming and the relative depths of underlying source sills are also indicated.

Sector 1, northwest of the study area, comprises 20 HTVCs located below the Top Tang Formation. There are three columns of seismic dimming above eye structures; one column from Top Tare upwards through the Brygge Formation and above a high-amplitude anomaly within the Tare Formation, one column from Top Tang to Top Tare Formation, and the third column from the Top Tare Formation upwards through the Brygge Formation. High-amplitude anomalies are present above six HTVCs, which are fed by sills occurring at unequal depths in Cretaceous strata. There is one example of a deeply buried crater with an overlying eye structure (Figure 8b), interpreted to indicate reutilisation of an existing hydrothermal conduit by overpressured hydrothermal fluids to form another HTVC.

Of the 24 HTVCs interpreted in Sector 2, in the northeast of the study area, all but four are associated with the Top Tang Formation, with eye-shaped HTVCs and dome structures distributed above and below the Top Tang Formation. There are high-amplitude anomalies in the Brygge formation above eleven (11) HTVCs, and all of these HTVCs are fed from deep-seated sills. The seismic amplitude of the Brygge formation shows great lateral variation, and is in places typically not associated with HTVCs. This means such amplitude anomalies could be lithological or due to shallow fluid

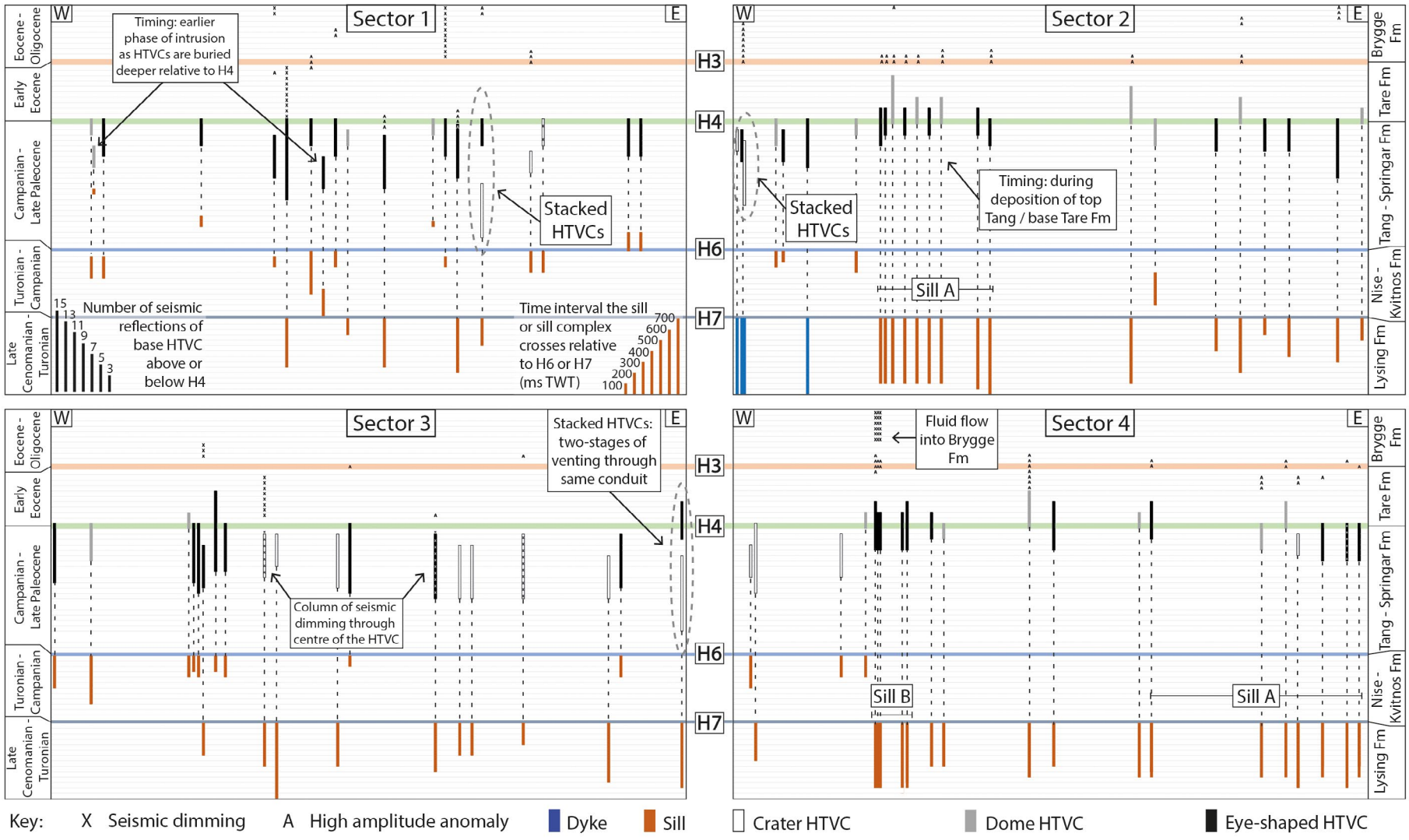

FIGURE 9 Plots showing the relative timing of formation of HTVCs and associated high-amplitude anomalies (A), seismic dimming (X) and underlying source sills, in the four sectors of the study area. HTVCs are plotted from their base, in number of seismic reflections relative to horizon H4, whilst high-amplitude anomalies and seismic dimming are plotted relative to horizon H3. For sills, every horizontal interval represents 50 ms TWT thickness. Sector 2 contains three interpreted dykes that feed the HTVCs (blue). Reference horizons are labelled: H3 (Top Tare Formation); H4 (Top Tang Formation); H6 (Top Nise Formation) and H7 (Top Lysing Formation), with ages labelled on the left-hand side and stratigraphic units on the right-hand side of the figure. Dotted lines connect HTVCs to their corresponding feeder sills

TABLE 1 Published ranges of diameter and height of hydrothermal vent complexes along the North Atlantic margin, with data added from this paper

Paper	Diameter, m	Height, m	Location
Planke et al. (2005)	400–11,000	30–450	Vøring and Møre Basins, offshore Norway, regional study
Reynolds et al. (2017)	700–11,000	36–504	Danmarkshavn and Thetis Basins, offshore NE Greenland
Omosanya, Maia, and Eruteya (2020)	516–3,945	77–600	Vøring Basin, offshore Norway
This paper	300–3,100	27–374	Modgunn Arch, south Vøring Basin, offshore Norway

processes. However, Figure 7c clearly shows an example of a soft, bright spot within the Brygge Formation, laterally restricted and located directly above an HTVC, interpreted to represent a gas pocket. This gas could have been fed from the pre-Cenozoic strata. This high-amplitude anomaly was interpreted and RMS amplitude extracted to show its limited lateral extent in plan view (Figure 10a,b). In addition, RMS amplitude was extracted between the Top Tare Formation (H3) and 10 ms TWT above H3, to show in plan view examples of where high-amplitude anomalies are located immediately above HTVCs (Figure 10c).

There is one example of stacked HTVCs whereby an eye-shaped HTVC is positioned within and just above a deeper crater structure (Figure 8c). We suggest that this hydrothermal conduit has been reutilised just after the crater was filled such that the uppermost crater fill was eroded during the formation of the overlying eye-shaped HTVC. No clearly resolved sill was interpreted as the source of this stacked HTVC and two nearby HTVCs, whilst seismic dimming and distortion is clear in a narrow, vertical pipe-like manner to the deeper parts of the basin (Figure 8c). It is possible that these are vertical dykes feeding the HTVCs, as opposed to sills. Dykes appear in seismic section as narrow, sub-vertical columns of chaotic or low amplitude seismic character, which may be traced in plan view as linear features (Thomson, 2007).

Sector 3, in the southwest of the study area, comprises craters located between two and six seismic reflections below the Top Tang Formation. Conversely, the eye-shaped HTVCs are closely associated with the Top Tang Formation, occurring either immediately below, or crossing into the Tare Formation. Despite being associated with the Top Tang Formation, the two domes show different timings of formation; the larger dome was formed during the deposition of the Tang Formation (e.g. Figure 7d), whereas the smaller dome formed on top of the Top Tang Formation during the deposition of the Tare Formation (e.g. Figure 7c). The plot in Figure 9 shows HTVCs at various seismic reflections below the Top Tang Formation, indicating several phases of magmatic activity and formation of HTVCs from the Paleocene to early Eocene. There is also evidence of one hydrothermal conduit terminating in a crater and overlying eye-shaped HTVC, a character suggesting that the hydrothermal conduit generating the crater was reutilised to form the eye structure above (Figure 8a). Two HTVCs show seismic dimming in the Tare and Brygge Formations, which may be indicative of gas escape in the past. There are also three high-amplitude anomalies within the Tare and Brygge Formations, which may indicate gas pockets at present day.

Sector 4, in the southeastern part of the study area, reveals HTVCs that are more closely related to the Top Tang Formation. Eight eye structures and six domes were formed at the very top of the Tang Formation, whilst four craters are found within the Tang Formation per se. Eleven (11) HTVCs are associated with high-amplitude anomalies in the Tare and lowermost Brygge Formations, whilst three eye structures are associated with high-amplitude anomalies at the Top Tare and base Brygge Formations. Seismic dimming is observed in the overlying Brygge Formation. All HTVCs with high-amplitude anomalies were fed from deep-seated sills (Figure 9).

From the 85 HTVCs identified in this work, 82 comprise hydrothermal conduits—three conduits terminate in stacked pairs of HTVCs and two of these pairs also show amplitude brightening in the Brygge Formation (Figure 8b,c), interpreted to indicate subsequent fluid flow. Combining the number of high-amplitude anomalies and seismic dimming above HTVCs gives a total of 35 hydrothermal conduits (43%) that are interpreted to have focused fluid flow after their initial formation. The eastern flank of the arch (the northeast and southeast sectors) contains 22 examples of HTVCs with overlying amplitude anomalies, where all 22 HTVCs were originally fed from deep-seated sills. The western flank of the arch (the northwest and southwest sectors) contains 13 examples of which six HTVCs were originally fed from medium-depth sills. It is interpreted that the majority of renewed fluid flow originates from the depths of the deepest sills in the basin (or even from deeper, lower crust sources) on the eastern flank of the Modgunn Arch, an area coinciding with a large arch-bounding fault associated with several deep-seated sills. The deepest sills feed 51 HTVC conduits, medium sills feed 25 and shallow sills feed five of the HTVC conduits, whilst dykes feed three HTVC conduits.

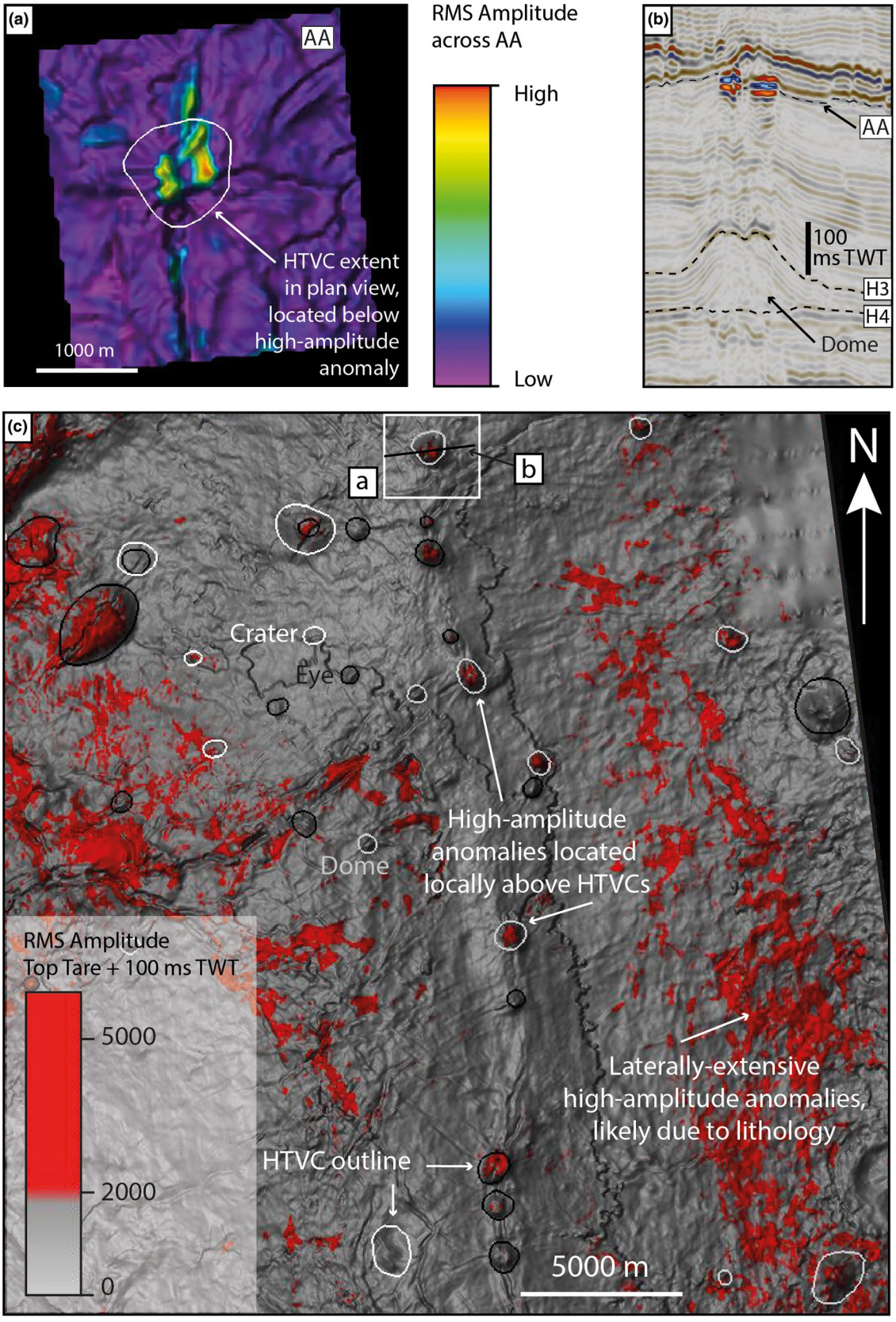

FIGURE 10 (a) Map view of the laterally restricted high-amplitude anomaly overlying a dome HTVC; (b) seismic section showing the HTVC and amplitude anomaly; c) Map view showing the location of a) and (b), and the distribution of high-amplitude anomalies within 100 ms TWT above the Top Tare Formation (H3), this is shown in (b). Some of the high-amplitude anomalies are local and located above HTVCs, whilst others are more extensive, likely due to lithological changes

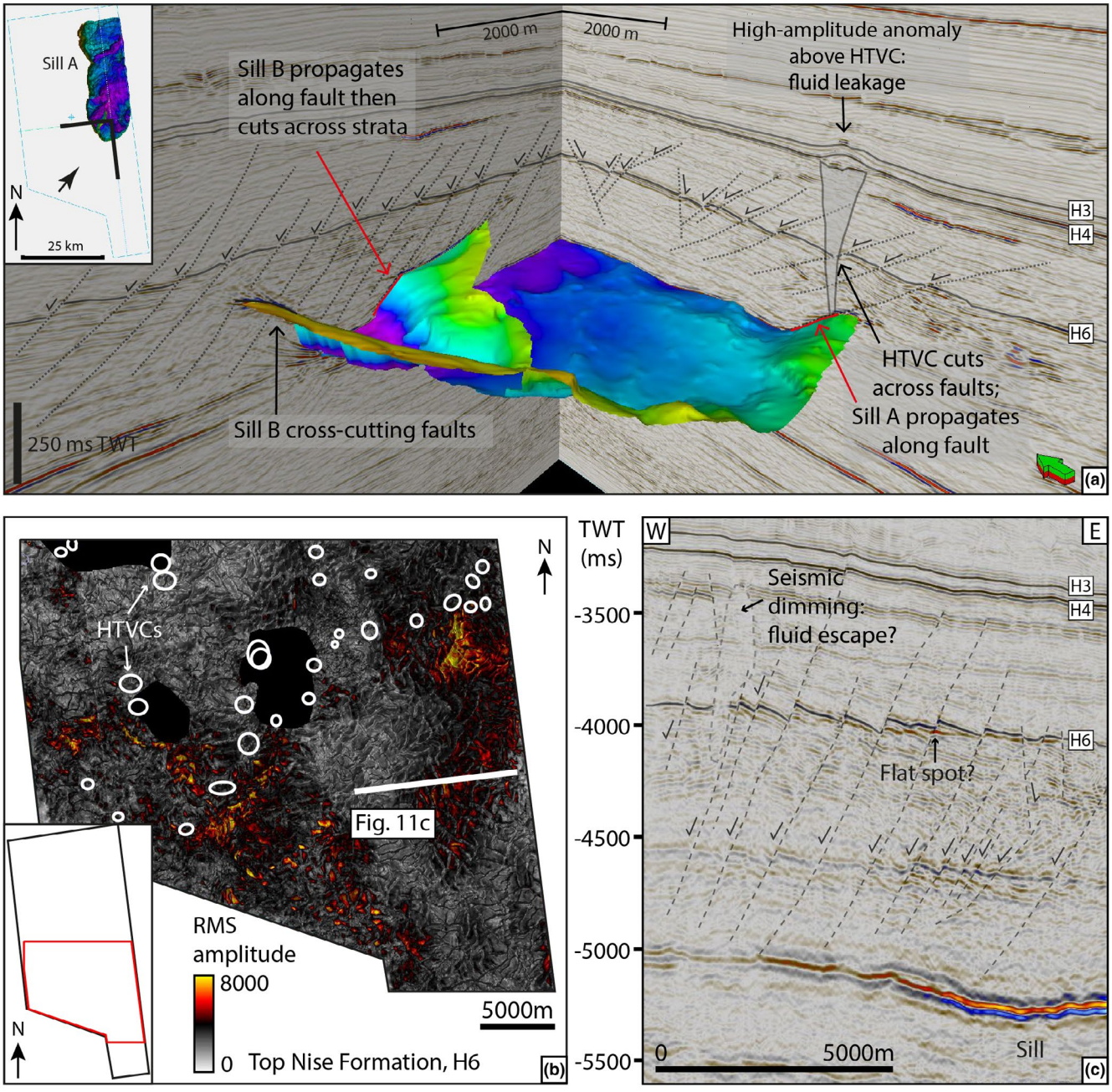

FIGURE 11 (a) 3D seismic representation of Sill A and B. Sill A cross-cuts faults and feeds a hydrothermal vent complex. Sill B cross-cuts faults to the southwestern limb and propagates along a fault on the northeastern limb of the Modgunn Arch. (b) Close-up map view of the RMS amplitude across the Top Nise Formation with location of seismic profile (c) indicated, where no hydrothermal vent complexes are interpreted. (c) Seismic dimming associated with the faulted Nise Formation, and a possible flat spot, both features suggesting fluid migration along faults

All of the HTVCs associated with Sill A (20 HTVCs) and Sill B (7 HTVCs) are located at the Top Tang horizon, whilst a few of the other sills which feed between 2 and 5 HTVCs each show slight differences in the number of reflections (−2 to −4) of the HTVC relative to the Top Tang horizon. This may reflect the lateral differences in deposition or erosion of sediments, or the feeder sill is actually a sill complex at depth where multiple sills intruded into the same area and it is not possible to differentiate between them—in addition, as noted by Manton (2015), there may be cases where two sills are feeding an HTVC.

Figure 5 also shows the diameter of the HTVCs coloured so as to highlight the HTVCs that were reutilised (in blue) against those that were not (in red). HTVCs ranging in diameter from 354 to 3,076 m are interpreted to have been reutilised; however, the majority of those reutilised have diameters greater than 700 m. This suggests that the larger HTVCs are more likely to be reutilised.

5.3 | High-amplitude anomalies within faulted Upper Cretaceous strata

The Nise Formation is clearly faulted throughout the study area (Figures 3 and 11). The uppermost Nise Formation contains localised high-amplitude anomalies ('flags') indicating that magmatic material or fluids migrated along the faults and are trapped in this unit. High-amplitude anomalies are particularly prevalent in the south-eastern parts of the study area, where the concentration of HTVCs is low (Figure 11b). These higher amplitudes may reflect local stratigraphic changes, such as the presence of sandstone stringers. However, there are instances of flags cross-cutting the faulted strata (Figure 11c).

In most cases, saucer-shaped sills (and where present, HTVC conduits) cross-cut Upper Cretaceous faults, whilst in other cases sills appear to propagate along these faults indicating that these faults can either be bypassed or utilised as magmatic and fluid migration pathways (Figure 11). Manton (2015) deduced that sills along fault planes have not been faulted, rather, some sills intruded along polygonal faults on the Modgunn Arch, although the majority of sills cross-cut the polygonal faults.

6 | DISCUSSION

6.1 | Timing and distribution of intrusions and fluid-flow features in the Modgunn Arch

Interpretation of a 3D seismic data set from the Modgunn Arch has revealed a complex arrangement of intrusive sills, hydrothermal vent complexes and fluid flow anomalies. Extrusive basalts were also emplaced on the continental crust at this time, but are not discussed here. The timing of formation of HTVCs is considered to coincide with the timing of sill intrusions. The sills intruded into Cretaceous strata, during continental breakup, whereas oceanic crust formed west of the study area. The intrusions rapidly heated the surrounding rocks, resulting in boiling of pore water and, in places, rapid maturation of organic material in the sill aureole (Jamtveit et al., 2004). As pressure cannot be dissipated quickly enough, the zones around the sill tips became overpressured and fracture networks formed along which gas, water and magmatic material escaped to the palaeo-surface. Fluid overpressure may also be generated during metamorphic dehydration reactions when various gases such as CO_2 and SO_2 are produced (Aarnes et al., 2010). Generation of large quantities of gaseous hydrocarbons such as CH_4 can result in overpressures large enough to trigger catastrophic blowouts and the formation

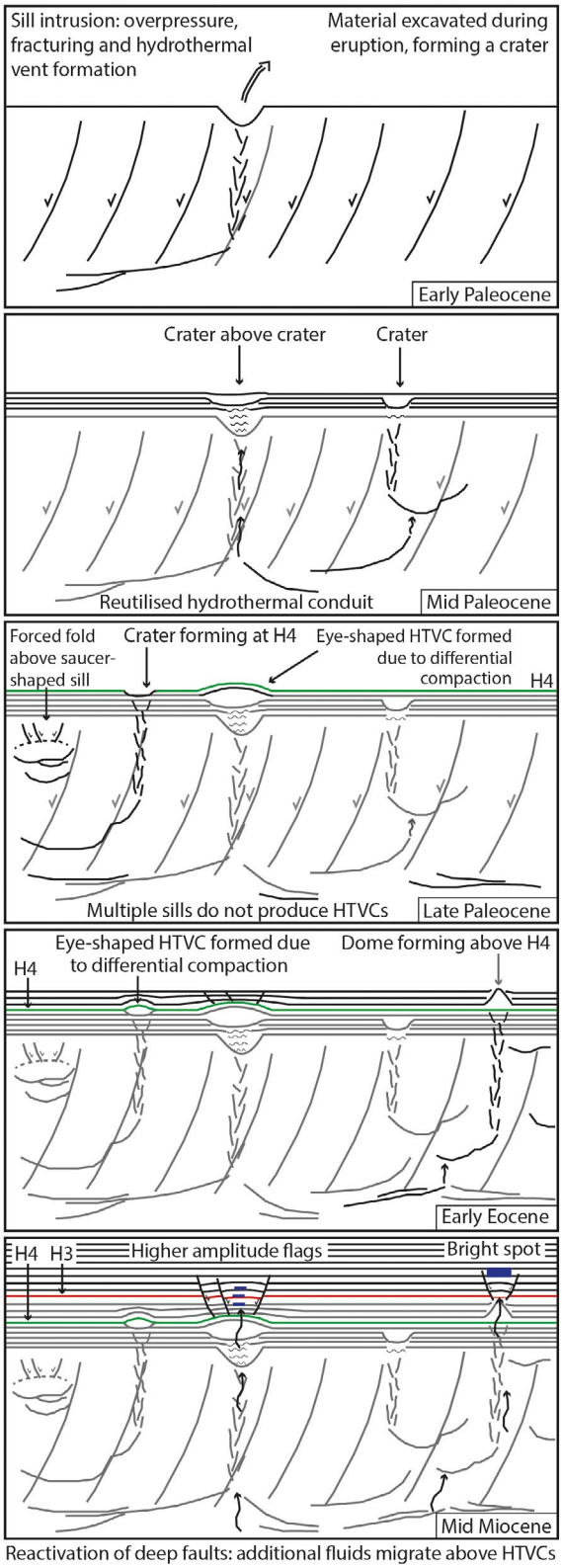

FIGURE 12 Schematic summary showing the key phases of Paleocene sill intrusion in the study area, and subsequent reutilisation of hydrothermal vent conduits for fluid flow. At least four phases of magmatic activity are interpreted, with additional fluid flow in the mid-Miocene. Diagram is not to scale

of HTVCs (Aarne, Podladchikov, & Svensen, 2012; Iyer et al., 2017). In some cases, HTVCs formed a crater where material was excavated, or a dome where material was intruded into shallow strata or extruded onto the palaeo-seafloor in a similar manner to a mud volcano. Eye-shaped HTVCs were also formed where some excavation and erosion of material occurred together with gas seepage into the sediments, inhibiting high levels of compaction and resulting in doming (Planke et al., 2005). Although it is still not well understood why these different HTVC structures form, it is clear that they are spatially correlatable with source sills below (Kjoberg et al., 2017; Planke et al., 2005; Schmiedel et al., 2017).

The intrusions of the North Atlantic Igneous Province, spanning eastern Greenland, parts of the United Kingdom, and Norway, are considered to have fed the methane and carbon dioxide gases that contributed to the temperature anomaly of the Paleocene-Eocene Thermal Maximum (PETM) (Reynolds et al., 2017; Svensen et al., 2004). The PETM is recorded between 55 and 55.8 Ma (Svensen et al., 2004), whilst this study reveals a more protracted intrusion of sills (and therefore expulsion of greenhouse gases) throughout the Paleocene to early Eocene. Planke et al. (2005) and Hansen (2006) showed in regional studies that there were two to three main episodes of igneous intrusion to form the North Atlantic Igneous Province. Whilst it is difficult to accurately distinguish between the timings of intrusion due to the reduced number of exploration wells crossing the Modgunn Arch, the inherent resolution limits of seismic data, and possible lateral differences in sedimentation rates, it is still apparent that several episodes of igneous intrusion occurred in the study area (Figure 9). Where wells and detailed stratigraphic data are available on the Norwegian Margin, the timing of sill intrusion can be well constrained. For example, biostratigraphic data combined with well-tie correlations revealed that the sill related to the Tulipan Field in the Møre Basin was emplaced during the earliest Eocene and was active for some time after, evidenced by the 100 m-thick transition zone seen in well 6302/6-1 (Kjoberg et al., 2017; Schmiedel et al., 2017). Furthermore, field studies in the North Atlantic Igneous Province have revealed the detailed characteristics of vent breccias and the relative timings of magmatic activity, which can be related to offshore subsurface examples in seismic data (Angkasa et al., 2017). Due to the presence of: (a) stacked HTVCs below the Top Tang Formation, (b) HTVCs immediately below the Top Tang Formation, and (c) dome HTVCs above the Top Tang Formation, we interpret at least four intrusion episodes, as illustrated schematically in Figure 12. Hamilton and Minshell (2019) also presented at least four phases of intrusions throughout the Paleocene and Early Eocene in the Faroe-Shetland Basin, which is part of the North Atlantic Igneous Province, to the south of the study area.

Three examples of 'stacked' HTVCs have been interpreted in this study, where a crater formed during the early Paleocene, followed by an eye-shaped HTVC. These are examples of hydrothermal conduits that have been reutilised for the rapid escape of hydrothermal fluids, as opposed to low-flux fluid seepage after the main eruptive event. Fluid seepage is interpreted from the presence of high-amplitude anomalies and also described by Svensen et al. (2003). For stacked HTVCs to occur, another sill must have intruded into the existing sill complex to heat the host rock and produce fluids in the same manner as the first intrusion. The fluids subsequently migrated along the established hydrothermal conduit with an explosive force to form another HTVC. One of the 'stacked' HTVC pairs may have been fed by a vertical dyke (Figure 8c), as no clear sills are imaged below, and although vertical dykes are also not imaged as bright reflections, they can subtly manifest as chaotic, low-amplitude seismic columns (Thomson, 2007). As seismic data resolution decreases with depth, particularly when imaging below basalt, an alternative explanation is that the HTVCs could have been fed directly from basement faults, or sills that are not seismically resolved. However, given how clearly other surrounding deep sills are imaged, it is interpreted that dykes are the source points for these HTVCs, which may be expected in such a setting. Skogseid et al. (1992) and Davies, Bell, Cartwright, and Shoulders (2002) also presented examples of dyke-fed volcanic vents or craters at the sea floor within the Vøring and Faeroe-Shetland Basins respectively; therefore, this is also expected to be the case on the Modgunn Arch.

High-amplitude anomalies and seismic dimming must always be interpreted with caution. Variations in cementation, pore fluid pressure, lithology, differential compaction, to name a few, can also cause a change in acoustic impedance contrast and result in amplitude anomalies (Harilal & Biswal, 2010). Seismic dimming may indicate that fluids have migrated along this pathway, possibly with patchy gas distributed in this zone, whilst high-amplitude anomalies may indicate the presence of a gas pocket at present time (Løseth, Gading, & Wensaas, 2009). High-amplitude anomalies are found across the study area, located above 39% of the HTVC conduits, that are mostly fed from deep sills, particularly on the eastern flank of the Modgunn Arch. Therefore, fluids fed primarily from deeper parts of the basin have migrated along sills and the HTVCs to overlying strata, at some point from the early Miocene, as amplitude anomalies are found across the Eocene to early Miocene-age strata. Other conduits that do not appear to be seeping may be sealed, or the seismic does not clearly show evidence of subsequent fluid flow (Figure 7e).

6.2 | Morphology and depth of sills sourcing HTVCs

The diameters of source sills found in this study area range from 1 to 18 km on average, with one sill extending north-south for at least 50 km, likely continuing beyond the study area (Figure 6). These are on-par with those found in field studies in the Karoo Basin, South Africa, where saucer-shaped sills in outcrop have diameters of up to 60 km (Polteau, Mazzini, Galland, Planke, & Malthe-Sørenssen, 2008). There is no clear correlation between the size of the sills and the presence of HTVCs, yet a greater proportion of the larger HTVCs are reutilised when compared to the smaller HTVCs (Figure 5). The larger the HTVC, the greater the amount of overpressure was required to form it; if the conduit is larger or more fractured, there may be a greater chance for later pulses of fluids to migrate along this pathway.

Only five of the mapped HTVCs appear to be fed from shallower depth sills. Aarnes et al., (2012) modelled the reaction-induced fluid overpressure build-up—such as that occurring in the metamorphic aureole of a sill intrusion—to constrain the conditions necessary to hydraulically fracture the overburden for pipe formation and focused fluid escape. They determined that decreasing host rock permeability is required for fracturing to occur with increasing intrusion depth, as opposed to fluid escape through the pore network. When heated, high total organic content values in the sediment (e.g. TOC, 1%–5%) will produce large volumes of methane gas that increase overpressure in such settings, although much higher TOC will decrease the tensile strength of the host rock and venting becomes less likely. Furthermore, heating due to sill intrusions will boil water already present in the rocks, which will also increase pore fluid pressure. For instance, Manton (2015) recorded 98 small (100–300 m across) vents directly above a shallow-depth sill on the Modgunn Arch, confirming that vents can be fed from shallow sills but these have not been analysed in this study. Planke et al. (2005) and Reynolds et al. (2017) found that the larger HTVCs are fed from deeper sills. The deepest sills in the study area are found to feed the greatest number of HTVCs, in part owing to their size; the largest (50 km diameter) sill alone feeds 20 HTVCs (Figure 6). The size of vents depends on the surrounding region or rock volume of overpressure accessed by the sill tip (Iyer et al., 2017). The medium-depth sills also feed HTVCs—although these sills are aerially smaller than the deeper sills or sill complexes, they are typically more saucer-shaped and cross-cut large volumes of rock strata. Saucer-shaped sills and transgressive sills with steep sides may channel fluids sub-vertically along the base sill-sediment interface to sill tips and fracture the overburden (Planke et al., 2005).

We propose that deep, vertical dykes feed three HTVC conduits in the north of the study area. Dykes are difficult to image in seismic data due to the vertical and narrow structure, in the same way as pipes, whilst sub-vertical or tilted dykes become more reflective (Løseth et al., 2011; Thomson, 2007).

6.3 | Implications of reutilising magmatic migration pathways in continental margins

The main implications of reutilising magmatic migration pathways are: (1) the preferential focusing of fluids and potentially hydrocarbons in post-HTVC strata; (2) the generation of migration pathways along faults and sills during long 'post-intrusion' periods; and (3) the local addition of heat to promote diagenesis in parts of the basin, impacting on the porosity and permeability of the strata.

The first postulate above considers that magmatic features are increasingly shown to provide additional fluid-focusing pathways in sedimentary basins. For example, the fracture zone around sills and dykes can often be of heightened permeability compared to the surrounding host strata, focusing fluid flow to shallower units (Rateau et al., 2013; Senger et al., 2017). If forced folds are created above saucer-shaped sills, this creates a possible trapping mechanism as evidenced by the Tulipan well in the outer Møre Basin, where a small gas discovery was recorded in a dome above a saucer-shaped sill (Holford et al., 2012; Kjoberg et al., 2017; Polteau et al., 2008; Schmiedel et al., 2017). Schmiedel et al. (2017) also showed that the dome above the Tulipan sill was formed by a combination of syn-sill-emplacement forced folding and post-emplacement differential compaction, the latter of which is an important mechanism for forming subtle traps for hydrocarbons (Ward, Alves, & Blenkinsop, 2018). This work also shows that hydrothermal vent complexes play an important role in controlling the plumbing system of a volcanic sedimentary basin. Hydrothermal fluids and hydrocarbons can migrate along pre-existing HTVCs that cross-cut kilometres of host strata into much shallower and younger units. An example of this is illustrated by Svensen et al. (2003), who interpreted continued seep carbonate growth for ~50 million years within Eocene-Pliocene sediments above a HTVC linked to a Paleocene-age sill in the Vøring Basin. They showed that HTVCs can act as long-lasting fluid flow paths to shallower units or the sea floor, as the carbon isotopes from the carbonates are isotopically light and thought to have been fed from hydrocarbons migrating from the deep parts of the basin across the HTVC into overlying strata. In addition, Hamilton and Minshell (2019) documented high-amplitude anomalies above HTVCs in the Faroe-Shetland Basin. They were able to use AVO analysis to show an increase of negative amplitudes with increasing offset, characteristic of low-impedance gas sandstones. A range of near- to long-offset seismic data was not available for this study

and could have been useful in further analyses of amplitude anomalies. However, Hamilton and Minshell (2019) also noted that the amplitude anomalies could be diagenetic or lithological, and direct sampling is often required to conclude their true nature.

The second aspect being discussed considers the presence of high amplitude 'flags' cross-cutting the Upper Cretaceous Nise Formation (Figure 11) as well as relatively higher amplitudes along the fault planes. Their presence supports the postulate that Cretaceous faults acted as fluid migration pathways, with fluids or magmatic material being trapped in sand units within the uppermost Nise Formation, or migrating to form shallower sills or flows. Sills intruding into pre-existing faults such as those in the Nise Formation cause the faults to dilate and fracture further, contributing to form an additional fluid focusing pathway that may have not been viable prior to magma intrusion. In most cases, imaged HTVC conduits cross-cut these faults. However, the fact that some saucer-shaped sills propagate along these faults increases the importance of taking into account these faults as fluid and magmatic pathways, particularly if the faults form structural traps suitable for hydrocarbons to accumulate. An example of this is the nearest hydrocarbon discovery to the study area, the 'Ellida' discovery in the southernmost part of the Helland Hansen Arch (Factpage6405/7-1, 2005). Well 6405/7-1 was drilled in 2003 by Statoil (now Equinor), ~80 km southeast of well 6403/6-1. The first level found with hydrocarbons was the Upper Cretaceous Nise Formation—the primary target of the well. The presence of oil stains in well 6403/6-1 suggests that hydrocarbons also migrated into the Nise Formation in the southern part of the Modgunn Arch, but have since been lost along the existing fault pathways or during tectonic reactivation that formed the Modgunn Arch. Sills have not been interpreted in the southern Helland Hansen Arch, therefore, it is possible that magmatic activity has hindered a potential petroleum system on the Modgunn Arch.

Amongst the two previous postulates, it should also be considered that if magma migrates along an existing fault and crystallises, the magma and additional diagenesis in the metamorphic aureole may 'plug' the fault zone, reducing its permeability and compartmentalising the basin further (Holford et al., 2012). The impact of magmatic features on hydrocarbons depends on the timing of magma intrusion; if hydrocarbons are already in place, magma intrusions can compartmentalise fields, form preferential fluid escape pathways, or, if the intrusions are stratigraphically below hydrocarbon accumulations, they may have no impact (Senger et al., 2017). In contrast, if hydrocarbons are yet to be produced or migrated, the intrusions will either form preferential migration pathways to shallower reservoirs or to the surface, hinder migration, or decrease the quality of potential reservoirs. Reservoir quality is reduced either by sills intruding into the reservoirs themselves, or by chemical diagenesis due to additional fluids migrating into the reservoirs or excessive heating, increasing the saturation of chemicals which precipitate as cement in the pore spaces (Aarnes, Svensen, Polteau, & Planke, 2011). As an example, Manton (2015) demonstrated that the Nise Formation placed controls on the intrusion of sills around the Modgunn Arch due to its greater sand content. Therefore, several sills propagated immediately below, or into the sandier layers, which would have been detrimental to reservoir properties.

Finally, Brekke (2000) discusses the tectonic evolution of the Vøring Basin, noting the presence of a fossilised Opal A-CT boundary. The Opal A-CT transition occurs during early diagenesis, as silica converts from Opal-A to Opal-CT. Resulting strata containing recrystalised Opal-CT has a greater impedance contrast and results in a hard bottom simulating reflector in seismic data (Neagu, Cartwright, Davies, & Jensen, 2010). The Opal A-CT transition is temperature dependent (Roaldset & He, 1995) and although the reflection cross-cuts a significant thickness of strata on the Modgunn Arch, it does not follow the sea floor reflection. Therefore, it is considered to be a 'fossilized' Opal A-CT reflection, that is, recording a higher-than-present geothermal gradient (Brekke, 2000). This timing coincides with the reactivation of the Jan Mayen Corridor, associated faulting, and the consequent formation of the Modgunn Arch (Brekke, 2000; Gómez & Vergés, 2005). It is possible to consider that this event instigated further fluid migration along basement faults, sills and HTVCs, which may explain the presence of high-amplitude anomalies in Eocene-Miocene strata (Figure 12). These fluids will have added local heat to the upper crust to fossilise the Opal A-CT boundary along the Modgunn Arch. Nevertheless, Song et al. (2020) also observed that the fossilised Opal A-CT traces the distribution of the deep, 50 km sill on the eastern flank of the Modgunn Arch and suggested a spatial correlation between the location of the intrusion and the Opal A-CT reflection. If renewed magmatic input was associated with the reactivation of the Jan Mayen Corridor, enhanced heat flow via conduction could have fossilised the Opal A-CT transition.

7 | CONCLUSIONS

Three-dimensional (3D) seismic data were used in this study to interpret the relative timing and spatial distribution of intrusions and associated hydrothermal vent complexes on the Modgunn Arch. As seismic resolution and imaging of magmatic features improves, the reliability of interpreting the presence and timing of formation of these fluid migration pathways improves. This is vital for assessing hydrocarbon plays or geothermal prospectivity in volcanic sedimentary

basins. Therefore, the main conclusions of this work are summarised as follows:

1. At least four phases of magmatic intrusions are interpreted by the diachroneity revealed by the hydrothermal vent complexes;
2. Three instances of stacked hydrothermal vent complexes are presented for the first time on the southern part of the Modgunn Arch, indicating preferential high energy fluid expulsion along an established hydrothermal vent conduit;
3. Hydrothermal vent complexes are acting as preferential fluid focusing pathways since the main magmatic fluid expulsion event during the Paleocene-Eocene;
4. Specifically, three dykes are interpreted to feed hydrothermal vent complexes, including one stacked hydrothermal vent complex pair, therefore, dykes are also reutilised migration pathways. Upper Cretaceous faults are both utilised and bypassed by magmatic intrusions and hydrothermal fluid flow;
5. Potential deep crustal faults may have been reactivated during the Middle Miocene to form the Modgunn Arch, which could have re-introduced fluids and heat into the upper crust. Therefore, this study shows how understanding the timing and distribution of hydrothermal vent complexes and magmatic features is crucial for exploration and is applicable to magma-rich continental margins around the world.

ACKNOWLEDGEMENTS

The work in this study was conducted during a PhD study undertaken as part of the Natural Environment Research Council (NERC) Centre for Doctoral Training (CDT) in Oil and Gas. It is sponsored by Cardiff University and the British Geological Survey (BGS) via the British University Funding Initiative (BUFI) grant number GA/16S/007, whose support is gratefully acknowledged. The authors thank Schlumberger for the Petrel licences provided to the 3D Seismic Lab—Cardiff University, and the Norwegian Petroleum Directorate (NPD) and Diskos for graciously granting them access to the seismic data used in this research. The support of the geophysics group of the Department of Geoscience and Petroleum at NTNU is greatly recognised for their access to their Petrel-ready project during Kamal's post-doctoral program. There are no conflicts of interest. We also thank the reviewers B. Manton, D. Jerram and S. Planke for their constructive comments, and A. Rotevatn for his editorial handling of the manuscript.

PEER REVIEW

The peer review history for this article is available at https://publons.com/publon/10.1111/bre.12507.

DATA AVAILABILITY STATEMENT

The data that support the findings are available from the Norwegian University of Science and Technology (NTNU). Restrictions apply to the availability of these data, which were used under license for this study. Data are available with permission of NTNU.

ORCID

Chantelle Roelofse https://orcid.org/0000-0001-8363-0080
Kamal'deen O. Omosanya https://orcid.org/0000-0001-8959-2329

REFERENCES

6403/6-1. (2008). Retrieved from Factpages, Norwegian Petroleum Directorate website: https://factpages.npd.no/factpages/Default.aspx?culture=no

6405/7-1. (2005). Retrieved from Factpages, Norwegian Petroleum Directorate website: https://factpages.npd.no/factpages/Default.aspx?culture=no

Aarnes, I., Planke, S., Trulsvik, M., & Svensen, H. (2015). Contact metamorphism and thermogenic gas generation in the Vøring and Møre basins, offshore Norway, during the Paleocene-Eocene thermal maximum. *Journal of the Geological Society*, *172*(5), 588–598. https://doi.org/10.1144/jgs2014-098

Aarnes, I., Podladchikov, Y., & Svensen, H. (2012). Devolatilization-induced pressure build-up: Implications for reaction front movement and breccia pipe formation. *Geofluids*, *12*(4), 265–279. https://doi.org/10.1111/j.1468-8123.2012.00368.x

Aarnes, I., Svensen, H., Polteau, S., & Planke, S. (2011). Contact metamorphic devolatilization of shales in the Karoo Basin, South Africa, and the effects of multiple sill intrusions. *Chemical Geology*, *281*(3–4), 181–194. https://doi.org/10.1016/j.chemgeo.2010.12.007

Alves, T. M. (2012). Scale-relationships and geometry of normal faults reactivated during gravitational gliding of Albian rafts (Espírito Santo Basin, SE Brazil). *Earth and Planetary Science Letters*, *331–332*, 80–96. https://doi.org/10.1016/j.epsl.2012.03.014

Angkasa, S. S., Jerram, D. A., Millett, J. M., Svensen, H. H., Planke, S., Taylor, R. A., … Howell, J. (2017). Mafic intrusions, hydrothermal venting and the basalt-sediment transition: Linking onshore and offshore examples from the north atlantic igneous province. *Interpretation*, *5*(3), 83–101. https://doi.org/10.1190/int-2016-0162.1

Bischoff, A., Nicol, A., Cole, J., & Gravley, D. (2019). Stratigraphy of architectural elements of a buried monogenetic volcanic system. *Open Geosciences*, *11*(1), 581–616. https://doi.org/10.1515/geo-2019-0048

Brekke, H. (2000). The tectonic evolution of the Norwegian Sea Continental Margin with emphasis on the Vøring and Møre Basins. *Geological Society, London, Special Publications*, *167*, 327–378. https://doi.org/10.1144/GSL.SP.2000.167.01.13

Brekke, H., Dahlgren, S., Nyland, B., & Magnus, C. (1999). The prospectivity of the Vøring and Møre basins on the Norwegian Sea continental margin. In A. J. Fleet, & S. A. R. Boldy (Eds.), *Petroleum Geology of Northwest Europe: Proceedings of the 5th Conference. Petroleum Geology* (pp. 261–274). London: Geological Society. https://doi.org/10.1144/0050261

Bryan, S. E., & Ernst, R. E. (2008). Revised definition of Large Igneous Provinces (LIPs). *Earth-Science Reviews*, *86*(1–4), 175–202. https://doi.org/10.1016/j.earscirev.2007.08.008

Dalland, A., Worsley, D., & Ofstas, K. (1988).Bulletin 4 Mesozoic-Cenozoic Mid-Northern Norway.pdf.

Davies, R., Bell, B. R., Cartwright, J. A., & Shoulders, S. (2002). Three-dimensional seismic imaging of Paleogene dike-fed submarine volcanoes from the northeast Atlantic margin. *Geology*, *30*(3), 223–226. https://doi.org/10.1130/0091-7613(2002)030<0223:TDSIOP>2.0.CO;2

Deegan, C. E., & Scull, B. J. (1977).A proposed standard lithostratigraphic nomenclature for the central and northern North Sea. *Report of the Institute of Geological Sciences*.

Doré, A. G., Lundin, E. R., Fichler, C., & Olesen, O. (1997). Patterns of basement structure and reactivation along the NE Atlantic margin. *Journal of the Geological Society, London*, *154*, 85–92. https://doi.org/10.1144/gsjgs.154.1.0085

Duncan, L., Helland-Hansen, D., & Dennehy, C. (2009). The Rosebank Discovery. A new play type in intra basalt reservoirs of the North Atlantic volcanic province. In *6th European Production and Development Conference and Exhibition (DEVEX), Abstracts* (Vol. 1, p. 22). Aberdeen: Chevron Upstream Europe.

Franke, D. (2013). Rifting, lithosphere breakup and volcanism: Comparison of magma-poor and volcanic rifted margins. *Marine and Petroleum Geology*, *43*, 63–87. https://doi.org/10.1016/j.marpetgeo.2012.11.003

Gibb, F. G. F., & Kanaris-Sotiriou, R. (1988). The geochemistry and origin of the Faeroe-Shetland sill complex. *Geological Society Special Publication*, *39*(39), 241–252. https://doi.org/10.1144/GSL.SP.1988.039.01.22

Gómez, M., & Vergés, J. (2005). Quantifying the contribution of tectonics vs. differential compaction in the development of domes along the Mid-Norwegian Atlantic margin. *Basin Research*, *17*(2), 289–310. https://doi.org/10.1111/j.1365-2117.2005.00264.x

Hafeez, A., Planke, S., Jerram, D. A., Millett, J. M., Maharjan, D., & Prestvik, T. (2017). Upper paleocene ultramafic igneous rocks offshore mid-Norway: Re-interpretation of the vestbrona formation as a sill complex. *Interpretation*, *5*(3), 103–120. https://doi.org/10.1190/int-2016-0143.1

Hamilton, R. V., & Minshell, B. J. (2019). Hydrothermal vents and seismic anomalies: Implications for the petroleum system NE of Shetland. *Petroleum Geoscience*, *25*(1), 90–101. https://doi.org/10.1144/petgeo2017-072

Hansen, D. M. (2006). The morphology of intrusion-related vent structures and their implications for constraining the timing of intrusive events along the NE Atlantic margin. *Journal of the Geological Society*, *163*(5), 789–800. https://doi.org/10.1144/0016-76492004-167

Hansen, D. M., & Cartwright, J. (2006a). Saucer-shaped sill with lobate morphology revealed by 3D seismic data: Implications for resolving a shallow-level sill emplacement mechanism. *Journal of the Geological Society*, *163*(3), 509–523. https://doi.org/10.1144/0016-764905-073

Hansen, D. M., & Cartwright, J. (2006b). The three-dimensional geometry and growth of forced folds above saucer-shaped igneous sills. *Journal of Structural Geology*, *28*(8), 1520–1535. https://doi.org/10.1016/j.jsg.2006.04.004

Harilal, X. & Biswal, S. (2010). Pitfalls in seismic amplitude interpretation: Lessons from Oligocene channel sandstones. *The Leading Edge, SEG*, *29*(4), 384–390. https://doi.org/10.1190/1.3378300

Hjelstuen, B. O., Eldholm, O., & Skogseid, J. (1999). Cenozoic evolution of the northern Voring margin. *GSA Bulletin*, *111*(12), 1792–1807.

Holford, S., Schofield, N., MacDonald, J., Duddy, I., & Green, P. (2012). Seismic analysis of igneous systems in sedimentary basins and their impacts on hydrocarbon prospectivity: Examples from the southern Australian margin. *The APPEA Journal*, *52*(1), 229. https://doi.org/10.1071/aj11017

Holford, S. P., Schofield, N., & Reynolds, P. (2017). Subsurface fluid flow focused by buried volcanoes in sedimentary basins: Evidence from 3D seismic data, Bass Basin, offshore southeastern Australia. *Interpretation*, *5*(3), SK39–SK50. https://doi.org/10.1190/int-2016-0205.1

Iyer, K., Schmid, D. W., Planke, S., & Millett, J. (2017). Modelling hydrothermal venting in volcanic sedimentary basins: Impact on hydrocarbon maturation and paleoclimate. *Earth and Planetary Science Letters*, *467*, 30–42. https://doi.org/10.1016/j.epsl.2017.03.023

Jaeger, J. C. (1958). The solidification and cooling of intrusive sheets. In *Dolerites, a symposium* (pp. 77–87). Tasmania Univ. Geol. Dept.

Jamtveit, B., Svensen, H., Podladchikov, Y. Y., & Planke, S. (2004). Hydrothermal vent complexes associated with sill intrusions in sedimentary basins. *Geological Society, London, Special Publications*, *234*(1), 233–241. https://doi.org/10.1144/gsl.sp.2004.234.01.15

Kjoberg, S., Schmiedel, T., Planke, S., Svensen, H. H., Millett, J. M., Jerram, D. A., … Helsem, A. (2017). 3D structure and formation of hydrothermal vent complexes at the Paleocene-Eocene transition, the Møre Basin, mid-Norwegian margin. *Interpretation*, *5*(3), SK65–SK81. https://doi.org/10.1190/INT-2016-0159.1

Lockett, G. (2018). Geothermal power: An alternate role for redundant North Sea platforms? Retrieved from Offshore Magazine website: https://www.offshore-mag.com/pipelines/article/16762144/geothermal-power-an-alternate-role-for-redundant-north-sea-platforms

Løseth, H., Gading, M., & Wensaas, L. (2009). Hydrocarbon leakage interpreted on seismic data. *Marine and Petroleum Geology*, *26*, 1304–1319. https://doi.org/10.1016/j.marpetgeo.2008.09.008

Løseth, H., Wensaas, L., Arntsen, B., Hanken, N. M., Basire, C., & Graue, K. (2011). 1000 M long gas blow-out pipes. *Marine and Petroleum Geology*, *28*(5), 1040–1060. https://doi.org/10.1016/j.marpetgeo.2010.10.001

Lundin, E., & Doré, A. G. (2002). Mid-Cenozoic post-breakup deformation in the "passive" margins bordering the Norwegian-Greenland Sea. *Marine and Petroleum Geology*, *19*(1), 79–93. https://doi.org/10.1016/S0264-8172(01)00046-0

Manton, B. M. (2015). *The mechanics of sill propagation and associated venting, investigated using 3D seismic data from Offshore Norway* (PhD dissertation). Cardiff: Cardiff University. Retrieved from https://www.researchgate.net/publication/339208100

Miles, A., & Cartwright, J. (2010). Hybrid flow sills: A new mode of igneous sheet intrusion. *Geology*, *38*(4), 343–346. https://doi.org/10.1130/G30414.1

Neagu, R. C., Cartwright, J., Davies, R., & Jensen, L. (2010). Fossilisation of a silica diagenesis reaction front on the mid-Norwegian margin. *Marine and Petroleum Geology*, *27*(10), 2141–2155. https://doi.org/10.1016/j.marpetgeo.2010.09.003

Omosanya, K. O., Eruteya, O. E., Siregar, E. S. A., Zieba, K. J., Johansen, S. E., Alves, T. M., & Waldmann, N. D. (2018). Three-dimensional (3-D) seismic imaging of conduits and radial faults associated with hydrothermal vent complexes (Vøring Basin, Offshore Norway). *Marine Geology*, *399*(2017), 115–134. https://doi.org/10.1016/j.margeo.2018.02.007

Omosanya, K. O., Maia, A. R., & Eruteya, O. E. (2020). Seismic, morphologic and scale variabilities of subsurface pipes and vent complexes in a magma-rich margin. *Bulletin of Volcanology*, *82*, 40. https://doi.org/10.1007/s00445-020-01379-3

Planke, S., Rasmussen, T., Rey, S. S., & Myklebust, R. (2005).Seismic characteristics and distribution of volcanic intrusions and hydrothermal vent complexes in the Vøring and Møre basins.In A. G. Doré, & B. A. Vining (Eds.), *Petroleum Geology: North-West Europe and Global Perspectives - Proceedings of the 6th Petroluem Geology Conference* (pp. 833–844). London: Geological Society.

Planke, S., Svensen, H., Myklebust, R., Bannister, S., Manton, B., & Lorenz, L. (2015). Geophysics and remote sensing. In C. Breitkreuz & S. Rocchi (Eds.), *Physical geology of shallow magmatic systems*, Advances in Volcanology (An Official Book Series of the International Association of Volcanology and Chemistry of the Earth's Interior) (pp. 131–146). Cham: Springer. https://doi.org/10.1007/11157

Polteau, S., Mazzini, A., Galland, O., Planke, S., & Malthe-Sørenssen, A. (2008). Saucer-shaped intrusions: Occurrences, emplacement and implications. *Earth and Planetary Science Letters*, *266*(1–2), 195–204. https://doi.org/10.1016/j.epsl.2007.11.015

Rateau, R., Schofield, N., & Smith, M. (2013). The potential role of igneous intrusions on hydrocarbon migration, West of Shetland. *Petroleum Geoscience*, *19*(3), 259–272. https://doi.org/10.1144/petgeo2012-035

Reynolds, P., Planke, S., Millett, J. M., Jerram, D. A., Trulsvik, M., Schofield, N., & Myklebust, R. (2017). Hydrothermal vent complexes offshore Northeast Greenland: A potential role in driving the PETM. *Earth and Planetary Science Letters*, *467*, 72–78. https://doi.org/10.1016/j.epsl.2017.03.031

Roaldset, E., & He, W. (1995).Silica-phase transformation of opal-A to opal-CT to quartz - An experimental approach.Trondheim.

Rohrman, M. (2007). Prospectivity of volcanic basins: Trap delineation and acreage de-risking. *AAPG Bulletin*, *91*(6), 915–939. https://doi.org/10.1306/12150606017

Schmiedel, T., Kjoberg, S., Planke, S., Magee, C., Galland, O., Schofield, N., & Jackson, C. (2017). Mechanisms of overburden deformation associated with the emplacment of the Tulipan sill, mid-Norwegian margin. *Interpretation*, *5*(3), SK23–SK38.

Schofield, N., Holford, S., Millett, J., Brown, D., Jolley, D., Passey, S. R., … Stevenson, C. (2017). Regional magma plumbing and emplacement mechanisms of the Faroe-Shetland Sill Complex: Implications for magma transport and petroleum systems within sedimentary basins. *Basin Research*, *29*(1), 41–63. https://doi.org/10.1111/bre.12164

Senger, K., Millett, J., Planke, S., Ogata, K., Eide, C. H., Festøy, M., … Jerram, D. A. (2017). Effects of igneous intrusions on the petroleum system: A review. *First Break*, *35*, 1–10.

Skogseid, J., Pedersen, T., Eldholm, O., & Larsen, B. T. (1992). Tectonism and magmatism during NE Atlantic continental break-up: The Vøring Margin. *Geological Society, London, Special Publications*, *68*(1), 305–320. https://doi.org/10.1144/gsl.sp.1992.068.01.19

Smallwood, J. R., & Maresh, J. (2002). The properties, morphology and distribution of igneous sills: Modelling, borehole data and 3D seismic from the Faroe-Shetland area. *Geological Society Special Publication*, *197*, 271–306. https://doi.org/10.1144/GSL.SP.2002.197.01.11

Song, J., Alves, T., Omosanya, K., & Ze, T. (2020). Tectonic evolution of strike-slip zones on continental margins and their impact on the development of submarine landslides (Storegga Slide, northeast Atlantic). *Geological Society of America Bulletin*. https://doi.org/10.1130/B35421.1

Stagpoole, V., & Funnell, R. (2001). Arc magmatism and hydrocarbon generation in the Northern Taranaki Basin, New Zealand. *Petroleum Geoscience*, *7*(3), 255–267. https://doi.org/10.1144/petgeo.7.3.255

Stimac, J., Goff, F., & Goff, C. J. (2015). Intrusion-related geothermal systems. In *The encyclopedia of volcanoes* (2nd ed., pp. 799–822). Academic Press. https://doi.org/10.1016/b978-0-12-385938-9.00046-8

Svensen, H., Jamtveit, B., Planke, S., & Chevallier, L. (2006). Structure and evolution of hydrothermal vent complexes in the Karoo Basin, South Africa. *Journal of the Geological Society*, *163*(4), 671–682. https://doi.org/10.1144/1144-764905-037

Svensen, H., Planke, S., & Corfu, F. (2010). Zircon dating ties NE Atlantic sill emplacement to initial Eocene global warming. *Journal of the Geological Society*, *167*(3), 433–436. https://doi.org/10.1144/0016-76492009-125

Svensen, H., Planke, S., Jamtveit, B., & Pedersen, T. (2003). Seep carbonate formation controlled by hydrothermal vent complexes: A case study from the Vøring Basin, the Norwegian Sea. *Geo-Marine Letters*, *23*(3–4), 351–358. https://doi.org/10.1007/s00367-003-0141-2

Svensen, H., Planke, S., Maithe-Sørensen, A., Jamtveit, B., Myklebust, R., Eidem, T. R., & Rey, S. S. (2004). Release of methane from a volcanic basin as a mechanism for initial Eocene global warming. *Nature*, *429*(6991), 542–545. https://doi.org/10.1038/nature02566

The 2014 NPD lithostratigraphic charts. (2014). Retrieved from Norwegian Petroleum Directorate website: https://www.npd.no/en/facts/geology/lithostratigraphy/

Thomson, K. (2007). Determining magma flow in sills, dykes and laccoliths and their implications for sill emplacement mechanisms. *Bulletin of Volcanology*, *70*(2), 183–201. https://doi.org/10.1007/s00445-007-0131-8

Underhill, J. (1998). Jurassic. In K.W. Glennie (ed.), *Petroleum geology of the North Sea: Basic concepts and recent advances* (4th ed., pp. 245–293). Blackwell Science Ltd.

Ward, N. I. P., Alves, T. M., & Blenkinsop, T. G. (2018). Differential compaction over Late Miocene submarine channels in SE Brazil: Implications for trap formation. *Bulletin of the Geological Society of America*, *130*(1–2), 208–221. https://doi.org/10.1130/B31659.1

White, R., & McKenzie, D. (1989). Magmatism at rift zones: The generation of volcanic continental margins and flood basalts. *Journal of Geophysical Research*, *94*(B6), 7685–7729. https://doi.org/10.1029/JB094iB06p07685

How to cite this article: Roelofse C, Alves TM, Omosanya KO. Reutilisation of hydrothermal vent complexes for focused fluid flow on continental margins (Modgunn Arch, Norwegian Sea). *Basin Res*. 2020;00:1–25. https://doi.org/10.1111/bre.12507

APPENDIX A

TABLE A1 Table summarising the seismic stratigraphy of the Modgunn Arch

Seismic Units	Age of base	TWT Thickness (ms)	Internal character, geometry and terminations	Probable lithology (Dalland et al., 1988)	Seismic horizons
1	Pliocene	0–200	Chaotic internal strata, bound by an irregular sea floor and relatively planar base	Mass-transport deposit	H0-H1
2	Miocene	0–250	Wedge of planar strata with internal onlapping geometries; displaced by a shallow tier of faults which also extend to Unit 3	Deep-marine shale, with minor siltstones, sandstones and limestone stringers	H1-H2
3	Mid-Eocene	150–400	Faulted by polygonal faults; unit contains abundant local onlap and truncation geometries, with discontinuous amplitudes ranging from seismic dimming to high amplitude, positive anomalies, often in association with underlying faults or HTVCs. Contains a positive amplitude seismic reflection which cross-cuts this unit in the northeast of the study area	Deep-marine shales; Positive amplitude seismic reflection which cross-cuts stratigraphy corresponds to a 'fossil' Opal-A-CT phase boundary (Brekke et al., 1999)	H2-H3
4	Late-Paleocene	50–100	Mostly planar seismic reflections, with local high-amplitude anomalies and onlap and thickness changes above HTVCs	Deep-marine shales, possibly with variable amounts of volcanic material such as tuff	H3-H4
5	Early-Paleocene	100–200	Mostly planar seismic reflections, with occasional onlap. Unit 5 contains HTVCs typically with chaotic internal seismic character, whilst external seismic reflections either onlap onto the HTVCs or are truncated against them, where they are erosional. High amplitude, planar transgressive, layer-parallel and saucer-shaped reflections are present at the base of this unit	Deep-marine shales; with minor sandstones and limestones. HTVCs consisting of remobilised mudstones and possibly magmatic material. High-amplitude reflections at the base are sills and flows	H4-H5
6	Upper Cretaceous	1,000–1,500	Mostly seismically transparent, with heavily faulted planar strata. Faults at least 1 s TWT displace this unit. High amplitude, mostly saucer-shaped reflections cross-cutting host strata are also present	Deep-marine calcareous shales, interbedded with minor carbonates and sandstone stringers. Saucer-shaped igneous intrusions cross-cut host stratigraphy	H5-H7
7	Lower Cretaceous – Late Jurassic?	>2,000	Mostly seismically transparent, with large faults displacing the poorly resolved strata. High-amplitude planar transgressive or layer-parallel reflections are evident	Marine shales, with interbedded submarine fan deposits. Deep sill complexes are present	H7 and deeper